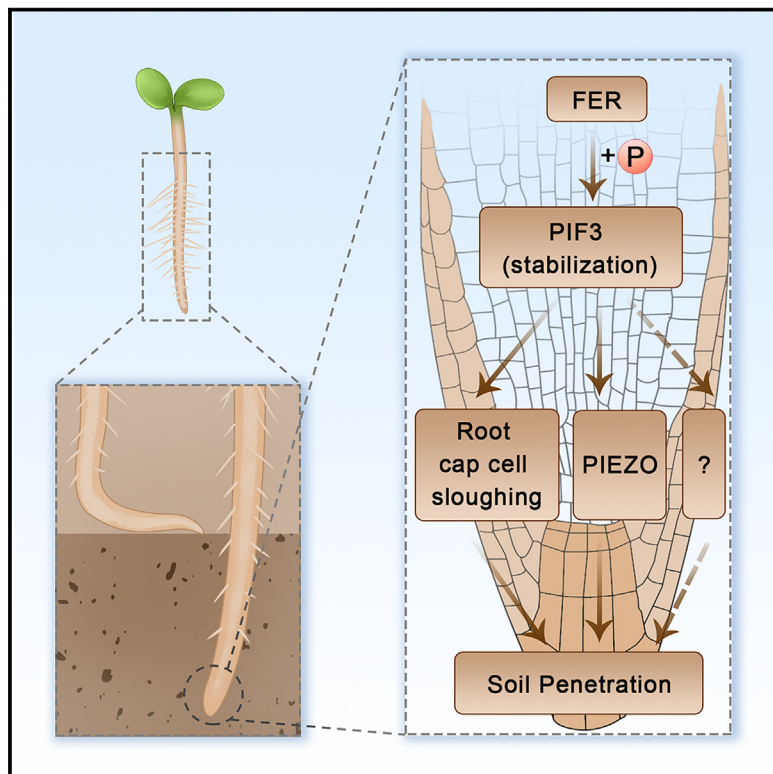


# Developmental Cell

## The soil emergence-related transcription factor PIF3 controls root penetration by interacting with the receptor kinase FER

### Graphical abstract



### Authors

Fan Xu, Jia Chen, Yingbin Li, ..., Xianming Fang, Kai He, Feng Yu

### Correspondence

feng\_yu@hnu.edu.cn

### In brief

Xu and Chen et al. report that the receptor kinase FERONIA interacts with, phosphorylates, and stabilizes the transcription factor PIF3 to regulate *PIEZO* expression in *Arabidopsis* root cap, which drives root penetration into soil.

### Highlights

- FER participates in *Arabidopsis* and soybean roots penetration into soil
- scRNA-seq profiling of *fer-4* root identified PIF3 as a FER-regulated target
- FER interacts with, phosphorylates, and stabilizes transcription factor PIF3
- FER-PIF3 module regulates *PIEZO* expression in *Arabidopsis* root cap



## Article

# The soil emergence-related transcription factor PIF3 controls root penetration by interacting with the receptor kinase FER

Fan Xu,<sup>1,4</sup> Jia Chen,<sup>1,4</sup> Yingbin Li,<sup>1</sup> Shilin Ouyang,<sup>1</sup> Mengting Yu,<sup>2</sup> Yirong Wang,<sup>1</sup> Xianming Fang,<sup>3</sup> Kai He,<sup>3</sup> and Feng Yu<sup>1,5,\*</sup>

<sup>1</sup>State Key Laboratory of Chemo/Biosensing and Chemometrics, College of Biology, and Hunan Key Laboratory of Plant Functional Genomics and Developmental Regulation, Hunan University, Changsha 410082, China

<sup>2</sup>College of Life Sciences, Hunan Normal University, Changsha 410081, China

<sup>3</sup>Ministry of Education Key Laboratory of Cell Activities and Stress Adaptations, School of Life Sciences, Lanzhou University, Lanzhou 730000, China

<sup>4</sup>These authors contribute equally

<sup>5</sup>Lead contact

\*Correspondence: feng\_yu@hnu.edu.cn

<https://doi.org/10.1016/j.devcel.2024.01.001>

## SUMMARY

The cotyledons of etiolated seedlings from terrestrial flowering plants must emerge from the soil surface, while roots must penetrate the soil to ensure plant survival. We show here that the soil emergence-related transcription factor PHYTOCHROME-INTERACTING FACTOR 3 (PIF3) controls root penetration via transducing external signals perceived by the receptor kinase FERONIA (FER) in *Arabidopsis thaliana*. The loss of FER function in *Arabidopsis* and soybean (*Glycine max*) mutants resulted in a severe defect in root penetration into agar medium or hard soil. Single-cell RNA sequencing (scRNA-seq) profiling of *Arabidopsis* roots identified a distinct cell clustering pattern, especially for root cap cells, and identified PIF3 as a FER-regulated transcription factor. Biochemical, imaging, and genetic experiments confirmed that PIF3 is required for root penetration into soil. Moreover, FER interacted with and stabilized PIF3 to modulate the expression of mechanosensitive ion channel PIEZO and the sloughing of outer root cap cells.

## INTRODUCTION

The seeds from angiosperms often start their life cycle in subterranean darkness and must synchronously modulate both their upward emergence from soil and their downward penetration into the soil. To protect the fragile shoot apical meristem (by nonexpanded cotyledons) and root meristem (by the root cap) from mechanical injury by soil particles, seedlings employ multiple systems to maintain cellular integrity, including mechanosensitive ion channels and the cell wall integrity (CWI) pathway. Light and ethylene signaling also regulate soil emergence by recruiting specific components. For example, the central repressor of light signaling CONSTITUTIVELY PHOTOMORPHOGENIC 1 (COP1) is critical for sensing soil depth above seedlings by regulating the abundance of ETHYLENE-INSENSITIVE 3 (EIN3), a master transcription factor (TF) in the ethylene pathway.<sup>1–3</sup> The pathway relying on TF PHYTOCHROME-INTERACTING FACTOR 3 (PIF3) is activated in etiolated cotyledons to ensure successful soil emergence.<sup>4</sup> However, although several studies have focused on the inability of the root to penetrate a substrate, it remains unknown whether soil emergence and root penetration share common components.

Roots forage the soil for nutrients to sustain growth. As they elongate through the soil, roots can encounter belowground ob-

stacles caused by drought and/or heterogeneous soil composition, which results in a lower growth rate, leading to reduced crop yields for the aboveground plant tissues.<sup>5</sup> The root tip is thought to perceive the mechanical resistance of the soil (called mechanosensing) and convert this information into biochemical and electrical signals<sup>6–8</sup> (called mechanotransduction). The root tip consists of the root cap, the root apical meristem, and the quiescent center. The root cap, comprising the columella and lateral root cap (LRC) cells,<sup>7</sup> offers physical protection to the root apical meristem behind it against mechanical impedance during root penetration into the soil. In addition, root hairs provide an anchor for the root tip and assistance for emerging from soil pores and for penetrating into compacted soil.<sup>9</sup> More cortical cells files and/or thicker cortical cells positively affect root penetration.<sup>10</sup> Root anatomical studies have shown that smaller cells in the outer cortical region in maize (*Zea mays*) roots are associated with increased root penetration into hard soil layers by stabilizing the root against compression and reducing the risk of buckling and collapse.<sup>11</sup> For instance, a multiseriate cortical sclerenchyma in maize and wheat (*Triticum aestivum*) improves root tensile strength and increases penetration ability in compacted soils.<sup>12</sup>

During soil penetration, root cells must maintain their mechanical integrity, which is determined by the CWI pathway and



mechanosensitive ion channels. Members of *Catharanthus roseus* receptor-like kinase 1-like (CrRLK1L) protein family participate in perceiving CWI and modulate root intracellular responses. One CrRLK1L member, FERONIA (FER), is involved in CWI signaling,<sup>13,14</sup> as FER is activated by the signals of pectin esterification level induced by growth and/or cell wall damage<sup>15–18</sup> and by the small peptides RAPID ALKALINIZATION FACTOR 1 (RALF1)<sup>19</sup> and RALF23.<sup>20</sup> The FER homologs ANXUR1 (ANX1), ANX2, Buddha's Paper Seal 1 (BUPS1), and BUPS2 form complexes with wall-anchored leucine-rich repeat extensins (LRX8, LXR9, and LXR11) in *Arabidopsis* (*Arabidopsis thaliana*) pollen and bind to RALF4 and RALF19 to sense alterations in the cell wall.<sup>21,22</sup> In pollen, CrRLK1L-mediated CWI signaling also involves mechanosensitive ion channels, such as MscS-Like8 (MSL8).<sup>23</sup> Besides CWI, FER also plays essential roles in root-related biological programs, such as the response to soil-borne diseases<sup>24</sup> and monitoring energy and nutrient availability.<sup>25,26</sup> Loss-of-function *fer* mutants (such as the *fer-4* allele) exhibit defects in root hair development<sup>25,27,28</sup> and have limited mechanosensitivity, resulting in an abnormal growth response to various mechanical stimuli.<sup>29</sup> In addition, *fer-4* roots acidify their surrounding growth medium faster than the wild type and develop longer roots than the wild type under blue light illumination that stimulates root growth.<sup>19</sup> Moreover, *fer-4* roots are insensitive to the inhibition of root growth normally triggered by the FER peptide ligand RALF1.<sup>19</sup> FER therefore acts as a regulator hub for root growth via linking external environmental signaling with internal cellular activity.<sup>14</sup> Based on these observations, we were curious about whether and how FER might sense mechanical stimuli to modulate root penetration into the soil.

In this study, we first confirmed that the *Arabidopsis fer-4* mutant shows defects in root penetration into hard soil, agar-solidified medium, and sand. We then conducted a single-cell RNA sequencing (scRNA-seq) analysis, which identified that *fer-4* root cells exhibit a distinct clustering profile compared with wild-type roots, especially for the cells with root hair and root cap identity. This transcriptome analysis allowed us to also identify several putative FER-regulated TFs, one of which being PIF3. A combination of biochemical, imaging, and genetic approaches confirmed that FER interacts with, phosphorylates, and stabilizes PIF3, which then modulates the expression of its target genes in the root cap, such as the mechanosensitive ion channel *PIEZO* and genes related to cell sloughing, to confer the capacity to penetrate soil.

## RESULTS

### FER participates in root penetration

We asked whether FER is involved in root penetration by growing seedlings for the wild-type Col-0 and the loss-of-function *fer-4* mutant<sup>27</sup> in soil (low physical barrier, 0.52–1.10 g/mL, 16.6–284.5 kPa) and sand (high physical barrier, 1.88 g/mL, 349.3 kPa, Figures S1A and S1B). Compared with Col-0, *fer-4* seedlings developed a shorter primary root in soil (Figures 1A and 1B). In addition, *fer-4* seedlings tended to show nonpenetrating roots that instead curved into the air or into the sand (bottom panel in Figure 1C), likely explaining the weak growth of these mutant seedlings under these conditions (upper panel in

Figures 1C and S1C). Based on these observations, we hypothesized that *fer-4* roots may have difficulty penetrating hard soil. To simulate the growth conditions of seedlings in hard soil conditions, we sowed Col-0 and *fer-4* seeds on the surface of half-strength Murashige and Skoog (MS) medium containing 1%, 1.5%, or 2% (w/v) agar (Figure 1D). We used the root penetrating rate into the medium as a readout for seedling adaptability to the mechanical constraints imposed by the growth milieu.<sup>30–32</sup> When grown on medium solidified with 1% agar, most Col-0 and *fer-4* roots were able to grow into the medium (>95%), with a slightly lower rate for *fer-4* (Figures 1D and 1E). As the agar concentration increased, the root penetrating rate declined in both genotypes (Figure 1E), indicating that a harder medium impedes root penetration. Importantly, the penetrating rate of *fer-4* roots was over 20% and 50% lower than that of Col-0 at 1.5% and 2% agar, respectively (Figures 1D and 1E). In addition, hard medium (2% agar) more severely inhibited primary root elongation (for medium-penetrating seedlings) in *fer-4* compared with Col-0 (Figure S1D). These results indicated that *fer-4* roots have a defect in penetrating harder medium. We confirmed this phenotype with the other allele *fer-5* (Figure S1L)<sup>27</sup> and a null *FER* mutant in the C24 accession, *sirène* (*srm*, Figure S1H).<sup>27,33</sup> In addition, a knockout mutant in LORELEI-LIKE-GPI-ANCHORED PROTEIN 1 (LLG1), *llg1-2*, lacking activity of a RALF coreceptor that works with FER,<sup>34</sup> also showed a defect in root penetration into harder medium (Figures S1I and S1J). We also tested whether FER function in regulating root penetration is conserved in other dicotyledons by quantifying the root penetrating rate of the two soybean (*Glycine max*) mutants *Gmlmm1-1* and *Gmlmm1-2*, which carry mutations in the *FER* paralog *LESION MIMIC MUTANT1*.<sup>35,36</sup> As with *fer-4*, *Gmlmm1-1* and *Gmlmm1-2* displayed a lower penetrating rate and a larger root cap, than their parental cultivar Williams82 (Figures 2A, 2B, and S2). In addition, when growing from uncompacted soil (0.52 g/mL, 16.6 kPa) to compacted soil (0.70 g/mL, 120.8 kPa), *Gmlmm1-1* showed a larger bending angle than Williams82, that is  $\theta_2 > \theta_1$  (Figure 2C), suggesting a defect for *Gmlmm1-1* in penetrating into compacted soil. We conclude that FER signaling plays an essential role in root penetration into soil.

Root adaptations to mechanical impedance comprise three possible strategies.<sup>8</sup> (1) At physiological level: increased mucilage production at the root tip and root cap cell sloughing to lubricate the root-soil interface.<sup>6</sup> (2) At the anatomical level, sharper root tip shapes decrease stress at the root tip via a more cylindrical cavity expansion.<sup>37,38</sup> At the morphological level, root hairs help root tip penetration by anchoring the root into the soil.<sup>9</sup> Therefore, the root architecture requires a strict spatiotemporal organization to influence root penetration ability.<sup>10</sup> We thus asked whether the defect in root penetration seen in *fer-4* is associated with its root architecture. *fer-4* seedlings had fewer and shorter root hairs<sup>25,27,28</sup> (Figure 3D), longer meristems with more cells (Figures 1F–1H), and a larger root cap (Figures 4B, S1F, and S1G) than those of Col-0. In addition, *fer-4* (Figure S1E) and *llg1-2* roots had a wider cortex and/or root diameter at the quiescent center position (Figure S1K). Collectively, *fer-4* shows defects in root penetration and displays an abnormal root architecture, hinting at a link between these two phenotypes.

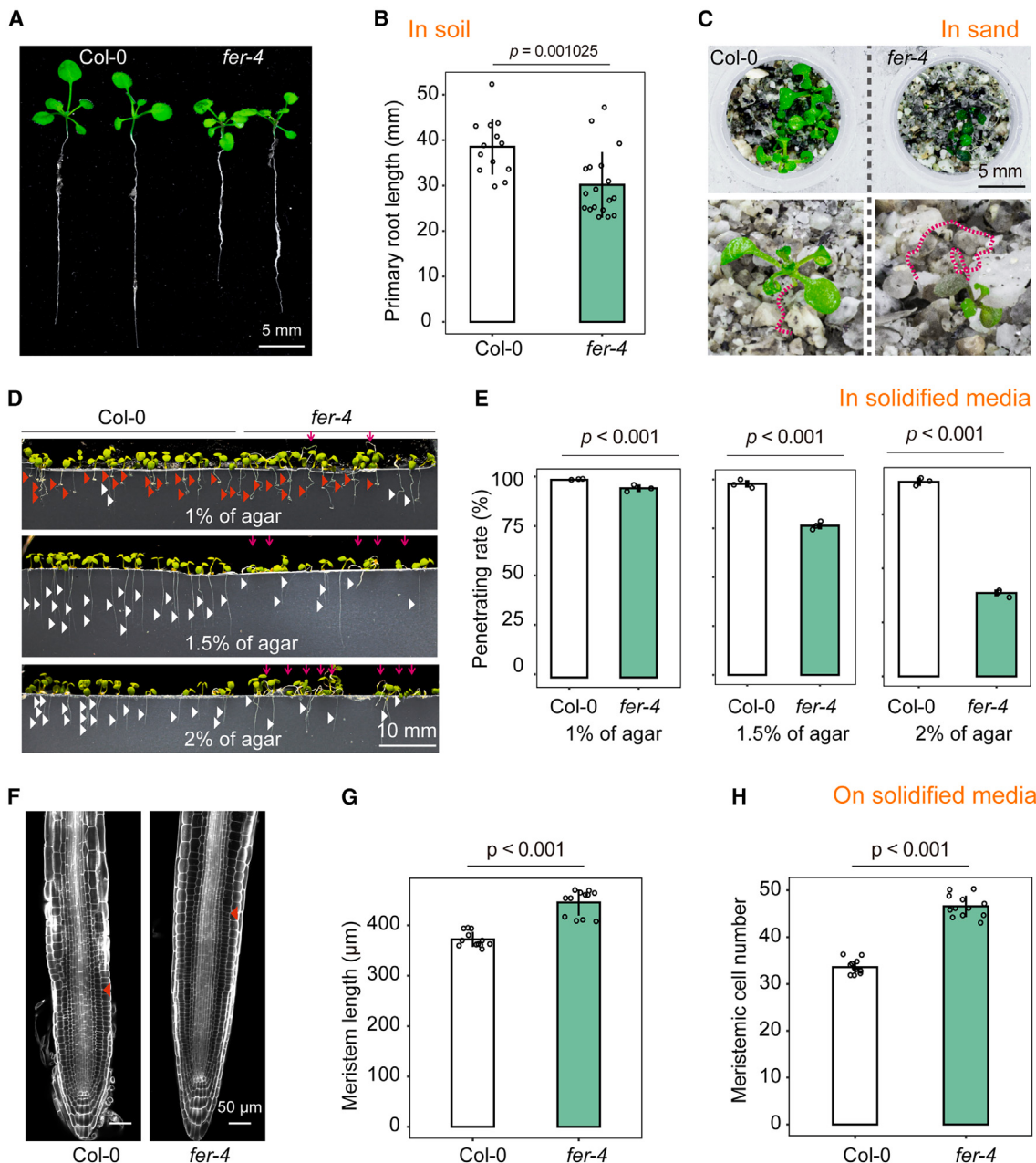


**Figure 1.** *fer-4* defects in root penetration into soil and root architecture

(A and B) 3-week-old Col-0 and *fer-4* seedlings grown in soil (A) and the length of their primary root (B).

(C) Representative image of 10-day-old Col-0 and *fer-4* seedlings grown on sand. The dashed magenta line indicates the root trajectory. See also Figure S1.

(D) Representative images showing the growth status of primary roots from 7-day-old Col-0 and *fer-4* seedlings grown on agar-solidified medium. The red and white triangles indicate helical and penetrating roots, respectively. The magenta arrows point to the seedlings with nonpenetrating root.

(E) Penetrating rate of Col-0 and *fer-4* roots in growth medium with different percentages of agar. Data are mean  $\pm$  SD ( $n = 3$  plates, >20 seedlings in each group).

(F) Root tips of 7-day-old Col-0 and *fer-4* seedlings grown on the surface of agar-solidified MS medium. Seedlings were stained with calcofluor white. The red triangle indicates the edge of the meristem.

(G and H) Meristem length (G) and number of root cortical meristematic cells (H) of the Col-0 and *fer-4* seedlings shown in (F). Data are mean  $\pm$  SD from three independent experiments ( $n > 15$  seedlings). At least three biological replicates in (A)–(H) were performed with similar results. For (B), (E), (G), and (H), p values were obtained by Student's t test comparing Col-0 and *fer-4*.

#### scRNA-seq analysis of Col-0 and *fer-4* roots

Root architecture and development correlate with root penetrating capacity.<sup>11,12,39</sup> To determine the molecular mecha-

nism(s) of FER in root penetration, we performed scRNA-seq of *fer-4* and Col-0 root tips. Accordingly, we treated 7-day-old Col-0 and *fer-4* seedlings with water (mock) or with 2  $\mu$ M

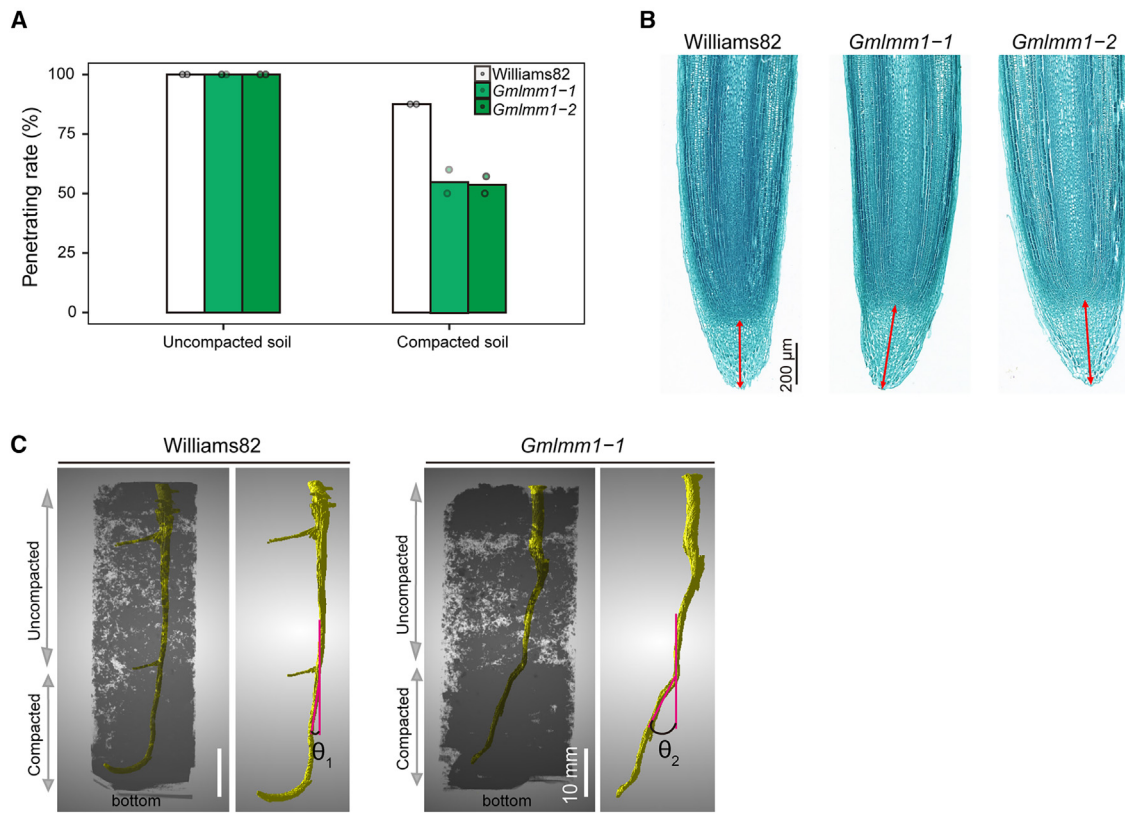


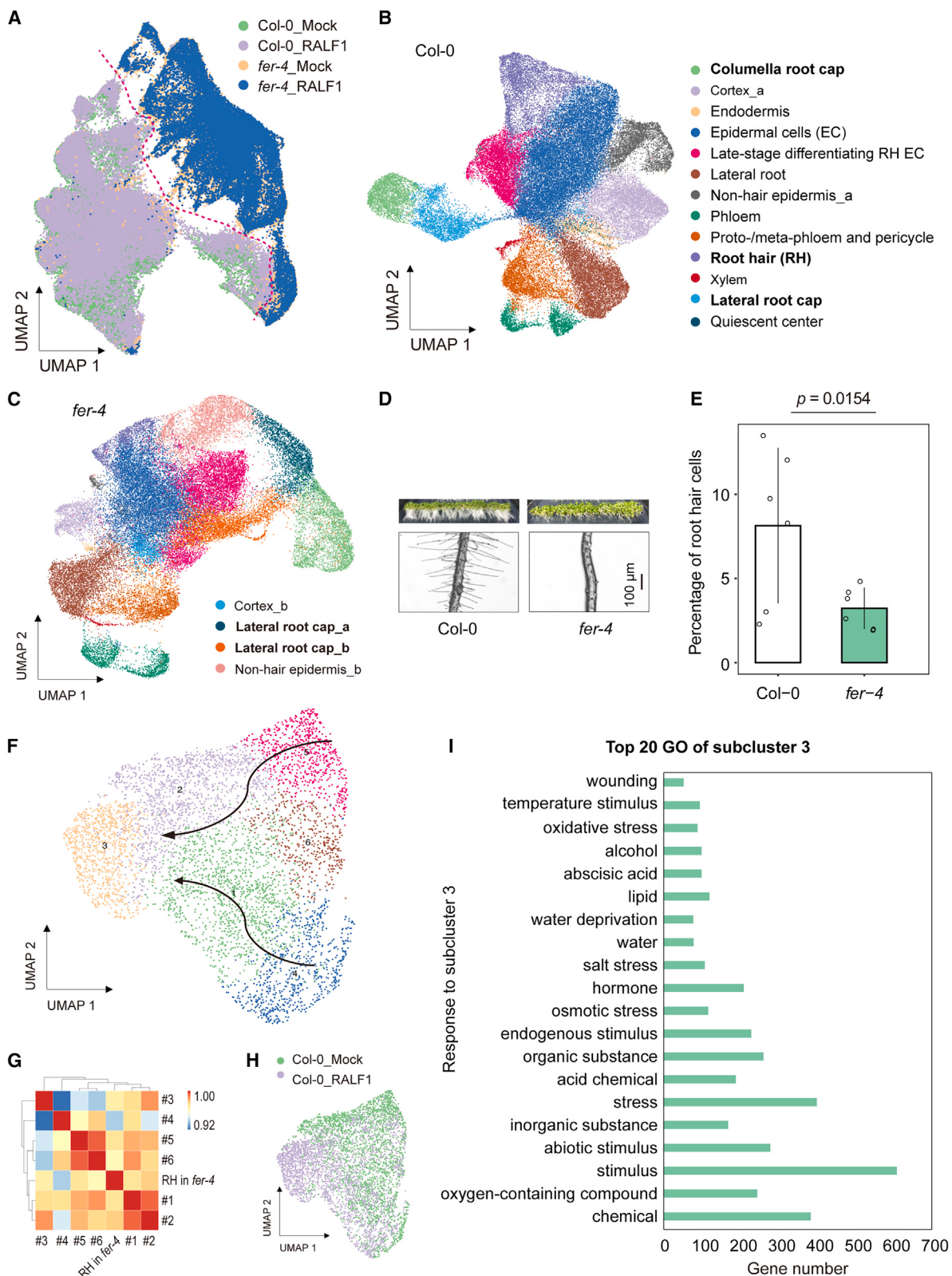
**Figure 2. Soybean fer-related mutants in the penetration assay and their root cap phenotype**

(A) Penetrating rate of soybean roots from seedlings grown on uncompacted (0.5 g/mL) or compacted (0.9 g/mL) soil. Rates from two biological replicates ( $n > 7$ ). (B) The *Gmlmm1-1* and *Gmlmm1-2* mutants have a larger root cap than the wild-type Williams82. The roots of 5-day-old soybean seedlings grown in soil were used for anatomical sections. The red lines with double arrows indicate the height of the root cap. See also Figure S2. (C) Computed tomography (CT) images showing the soybean root growing in compacted soil.  $\theta$  indicates the bending angle of the root when penetrating into the compacted soil (0.7 g/mL).

RALF1 (to activate FER) for 2 h, before isolating protoplasts for transcriptome analysis using the 10 $\times$  Genomics Chromium platform.<sup>40</sup> We detected approximately 2,430 expressed genes per cell, with more than 24,000 total genes across the cell population. We prefiltered the data at both cell and gene levels, resulting in a pool of 26,376 *fer-4* cells and 44,529 Col-0 cells used for analysis. We accounted for the effect of protoplasting on the transcriptome by regressing out the variations caused by protoplasting-induced genes,<sup>41</sup> which were removed from the analysis. After multiple quality control steps (see STAR Methods and Figure S3A), we conducted a cell-type annotation and cluster identification analysis. First, we uncovered 19 distinct clusters for the 12 samples of Col-0 and *fer-4* roots after principal-component analysis (PCA) and unsupervised analysis (Figure S3B). Importantly, the clustering pattern of *fer-4* cells was distinct from that of Col-0 based on their scRNA-seq profiles (Figure 3A). Second, we subjected the six samples from Col-0 roots and the six samples from *fer-4* roots to a separate clustering analysis using uniform manifold approximation and projection (UMAP, Figures 3B and 3C). Third, after assigning each cluster to their likely cell type based on the expression levels of known marker genes (Figure S3C),<sup>42,43</sup> we observed that nearly all major cell or tissue types present in the root were captured by

at least one cluster (Figures 3B and 3C). Notably, the *fer-4* samples showed distinct clustering for the cell types cortex (Cortex\_b) and non-hair epidermis (Non-hair epidermis\_b) from those obtained with Col-0 samples (Cortex\_a and Non-hair epidermis\_a, Figures 3B and 3C) via UMAP. Moreover, cells from the *fer-4* LRC (lateral root cap\_a/b) also showed a clustering pattern different from those of Col-0 root cap cells (LRC, Figures 3B and 3C), suggesting that FER is involved in the development of these tissues. Collectively, scRNA-seq profiling identified a developmental role for FER in the root, which is useful for determining the mechanism(s) of FER in root penetration.

In agreement with the root hair phenotype of *fer-4*, we captured fewer cells of *fer-4* with a root hair signature by scRNA-seq (Figures 3D and 3E). Root hair development can be divided into three phases: cell specification, initiation of bulge formation, and polarized tip growth.<sup>44</sup> Root hair development is associated with transcription and translation during cell specification, whereas stress responses and lipid biosynthesis occur at the late stage of polarized tip growth. To characterize root hair development at the transcript level, we selected the root hair cell type of Col-0 and sub-clustered it using UMAP (Figure 3F). We then used the differentially expressed genes (DEGs) obtained for each subcluster for a Gene Ontology (GO) analysis.

**Figure 3. Annotation of cell types from scRNA-seq results of Col-0 and fer-4 roots**

(A) UMAP representation of 12 samples from Col-0 and fer-4 root cells under mock conditions or treated with RALF1, colored by groups. Colors denote the corresponding genotype and treatment.

(legend continued on next page)

We determined that subclusters 4 and 5 represent the cell specification stage, while subcluster 3 matched the late stage (Figure 3G). We also plotted the six subclusters and extracted pseudotime information, which identified the developmental trajectory between subclusters, starting in subclusters 4 and 5 and ending in subcluster 3 (Figure 3F). To determine the stage of the *fer-4* root hairs, we conducted a correlation analysis between the expression profile of *fer-4* root hairs and the six subclusters from Col-0 root hairs. Based on scRNA-seq data, *fer-4* root hair appeared closer to subclusters 1 and 2, suggesting that FER is involved in root hair development and that most *fer-4* root hairs can enter the maturation stage without FER. Our previous study showed that RALF1, a ligand of FER, activates the FER signaling pathway to mediate root hair growth.<sup>25</sup> After a 2-h RALF1 treatment, the Col-0 root hair transcriptome displayed a clear difference relative to mock-treated root hairs, as evidenced by UMAP clustering (Figure 3H). GO analysis identified that RALF1 treatment alters the expression of genes in pathways related to stimulus (Figure 3I). These findings support the notion that the RALF-FER pathway mediates root hair growth, which is consistent with previous work<sup>25,27</sup> and validates our scRNA-seq approach. We thus exploited the scRNA-seq data in more detail to analyze the mechanism(s) by which FER affects root penetration.

### TFs and gene expression patterns are regulated by FER in the root cap

Given that the root cap is a key tissue in root penetration<sup>11,12,39</sup> and that *fer* mutants (*fer-4*, *Gmlmm1-1*, and *Gmlmm1-2*) had more cells in their root caps (for both the columella and LRC, Figure 4A) relative to their respective wild types, Col-0 and Williams 82 (Figures 2B, 4B, 4C, and S2), we focused on FER-regulated TFs in this tissue. To identify the primary TFs responsible for cell-type-specific DEGs between *fer-4* and Col-0, we predicted cell-type-specific TFs regulated by FER using the integrated gene regulatory network (iGRN)<sup>45</sup> and Paired Motif Enrichment Tool (PMET; Figures S4A–S4D).<sup>46</sup> The overlapping TFs defined by these two approaches are listed in Figure 4D. We identified 8, 15, and 11 overlapping TFs for the cell types columella root cap (CRC), lateral root cap\_a, and lateral root cap\_b, respectively (Figure 4D). Of these TFs, PIF3 and PIF4 were present in all three cell types, whereas MYC2, MYC3, and MYC4 were present in at least two cell types (Figure 4D). Notably, MYC2 physically interacts with FER and activates jasmonic acid signaling, thus negatively contributing to plant immunity,<sup>47</sup> in addition to cooperating with FER to regulate touch signaling in aerial tissues.<sup>48</sup> Mutants in MYC2 or related genes did not show a defect in root penetration into any of the agar-solidified media tested (Figure S4E), suggesting that MYCs have a negligible contribution to this phenotype. We thus focused on the roles of PIF3 in regulating gene expression in the root cap.

We investigated whether RALF1 affects gene expression in the root cap via PIF3 by identifying DEGs whose expression changed in response to RALF1 treatment in Col-0 and *fer-4* root cap cells (Figure 4E). In Col-0 CRC and LRC cells, we observed that dozens of genes are regulated by RALF1 treatment, whereas the same genes showed no change in expression in *fer-4* (Figure 4E), which was consistent with FER acting as a *bona fide* RALF1 receptor.<sup>19</sup> A comparison between RALF1-regulated DEGs and known PIF3-target genes (DEGs used to enrich for PIF3 in iGRN) yielded 14 (26.4% for PIF3-target genes) and 18 (13.4%) common DEGs in the CRC and LRC, respectively (Figure 4F). This result indicates that PIF3 is an important TF that modulates gene expression in the root cap.

### PIF3 controls root penetration by mediating root cap sloughing and the expression of mechanosensitive genes

To ascertain which of the potential TFs identified above act downstream of FER in the context of root penetration, we determined the penetration capacity of their corresponding mutants (Figure S4E). With the exception of *pif3* (Figure 5A) and *wrky38* mutants that displayed a lower penetrating rate than Col-0 when grown on medium solidified with 2% agar, the mutants *Arabidopsis response regulator 11* (*arr11*), related to *ap2.6* (*rap2.6*), *wrky45*, *dwarf and delayed flowering* (*ddf1*), and *zinc finger of Arabidopsis thaliana 6* (*zat6*) as well as the higher-order *myc* mutants *myc2myc3*, *myc2myc4*, *myc3myc4*, and *myc2-my2my3my4* showed penetrating rates comparable to those of Col-0 in medium solidified with 1%–2% agar (Figure S4E). Importantly, *pif3-1* roots showed a lower penetrating rate in 2% agar medium than Col-0 (Figure 5A) that was reminiscent of *fer-4*. In addition, *pif3-1*, like *fer-4*, had one additional cell layer in the CRC compared with Col-0 (Figures 5B and 5C). In addition, overexpressing *PIF3* in the *fer-4* background (*fer-4 PIF3-myc*) partially restored the CRC phenotype to that of the wild type (Figures S5A and S5B). The loss of PIF3 function (*fer-4 pif3-1*) did not show this effect (Figures S5A and S5B). A complementation line for the *pif3-1* mutant, *pPIF3::PIF3-Venus* in the *pif3-1* background (*pPIF3::PIF3-Venus* hereafter), displayed a normal penetrating rate and cell layer number in the CRC. Unlike *pif3-1*, *wrky38* showed a cell layer number in the CRC comparable to that of Col-0 (Figure S4F). Collectively, these data indicate that PIF3 is also required for root penetration.

Root cap sloughing helps protect roots as they penetrate the soil.<sup>49,50</sup> Higher levels of pectin methyl esterification of the cell wall attenuate the sloughing of the root cap outer layer by promoting cell-cell adhesion.<sup>51</sup> PIF3 regulates the expression of *Pectin Methyltransferase Inhibitors* genes (PMEIs, e.g., PMEI13 and PMEI7),<sup>52</sup> whose encoded proteins determine pectin methyl esterification levels in the cell wall. We therefore characterized the sloughing phenotypes of the root cap from Col-0, *fer-4*,

(B and C) UMAP representation of six Col-0 (B) and six *fer-4* (C) samples.

(D) Representative root hair phenotypes from Col-0 and *fer-4* seedlings grown on half-strength MS agar-solidified medium.

(E) Percentage of root hair cells in each scRNA-seq sample from Col-0 and *fer-4*. Data are mean ± SD. The p value was obtained by Student's t test.

(F) Sub-clustering of Col-0 root hair cell types. Arrows indicate developmental trajectory.

(G) Correlation analysis for root hair (RH) cells in *fer-4* and subclusters of root hair cell types in Col-0.

(H) Subcluster UMAP representation as in (B), colored by treatment.

(I) Gene Ontology (GO) term enrichment analysis for genes from the RALF1-dependent subcluster (#3). The top 20 terms are shown.

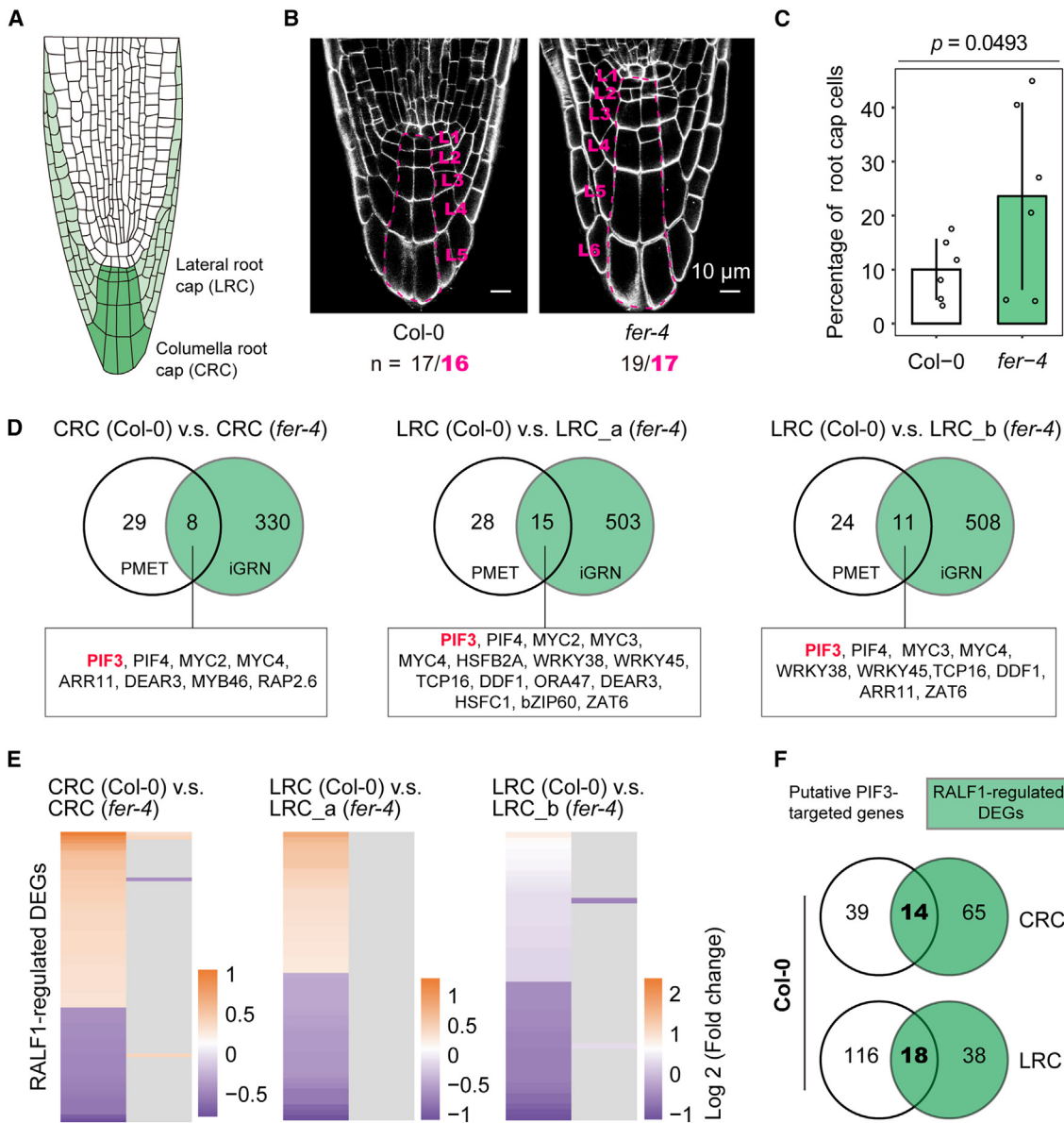


**Figure 4. Analysis of transcription factors that are regulated by FER**

(A) Diagram of the *Arabidopsis* root cap.

(B) Columella root cap in Col-0 and *fer-4*.

(C) Percentage of root cap cells in each scRNA-seq sample from Col-0 and *fer-4*. Data are mean  $\pm$  SD. The p value was obtained by Student's t test.

(D) Prediction of transcription factors regulated by FER in the columella and lateral root caps using PMET and iGRN approaches. See also Figure S4.

(E) Heatmap representation of the expression of RALF1-induced differentially expressed genes between Col-0 and *fer-4* in root cap cells.

(F) Venn diagram showing the number of overlapping DEGs between putative PIF3-target genes and RALF1-regulated genes. CRC, columella root cap; LRC, lateral root cap.

*pif3-1*, and *pPIF3::PIF3-Venus* seedlings. We defined three phases to describe the state of root cap sloughing: no sloughing, before sloughing, and ongoing sloughing. *fer-4* and *pif3-1* seedlings had more root caps in the before sloughing phase than Col-0 and *pPIF3::PIF3-Venus* seedlings (Figure 5D), which was consistent with the results of cell layer number in the CRC (Figures 5B and 5C). In contrast to *fer-4* and *pif3-1*, *pPIF3::PIF3-Venus* and Col-0 seedlings had a similar distribution of root cap sloughing at each phase (Figure 5D). Together, these re-

sults suggest that the outermost layer of the root cap in *fer-4* and *pif3-1* seedlings displays a defect in sloughing, which may be due to the higher cell-cell junction of their root cap cells, thus representing one strategy by which PIF3 controls root cap sloughing by regulating the expression of cell wall-remodeling genes.

Next, we asked whether the FER-PIF3 module regulates the expression of mechanosensitive genes. *PIEZO* is expressed in the root cap and is required for root penetration into hard medium,<sup>30,32,53</sup> prompting us to measure its expression levels in

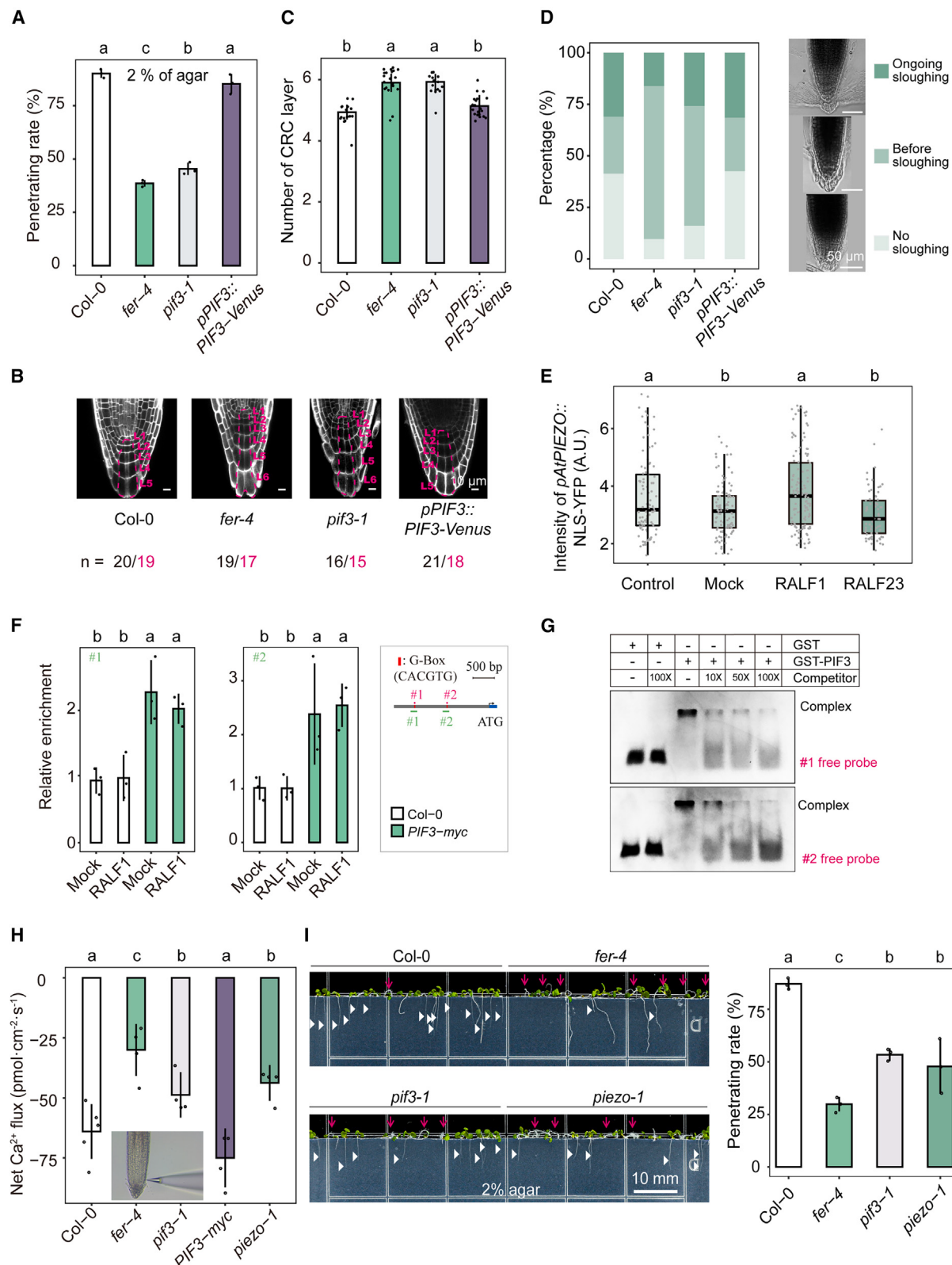


**Figure 5. PIF3 controls root penetration by mediating root cap sloughing and the expression of a mechanosensor gene**

(A) Root penetrating rate of Col-0, fer-4, pif3-1, and pPIF3::PIF3-Venus seedlings into medium solidified with 2% (w/v) agar. Data are mean ± SD ( $n = 3$  plates, >20 seedlings of each group).

response to RALF-mediated FER activation. For this purpose, we used a transgenic line expressing a construct encoding a nucleus-targeted yellow fluorescent protein (YFP) under the control of the *Arabidopsis PIEZO* promoter (*pAtPIEZO::NLS-YFP*).<sup>30</sup> We detected elevated YFP fluorescence in root cap cells upon treatment with RALF1, but not with RALF23 (Figure 5E), in relative to mock (water) and control (seedlings not transferred from solidified half-strength MS medium containing 1% agar). We also performed chromatin immunoprecipitation (ChIP) assays to assess PIF3 targeting to the *PIEZO* promoter, using the Col-0 as a negative control and *PIF3-myc* (in Col-0 background) lines as a test sample. PIF3-myc was enriched over *PIEZO* chromatin regions containing the G-box (CACGTG) elements in *PIF3-myc* but not in Col-0, suggesting that PIF3 binds to the *PIEZO* promoter *in vivo* (Figure 5F). We confirmed this result by electrophoretic mobility shift assay (EMSA) using recombinant glutathione S-transferase (GST)-tagged PIF3 (Figure 5G). These results indicate that PIF3 directly binds to the *PIEZO* promoter and regulates its transcription.

*PIEZO* changes the calcium ion ( $\text{Ca}^{2+}$ ) flux in the root cap.<sup>30</sup> Similar to *piezo-1*, both *fer-4* and *pif3-1* displayed weaker net  $\text{Ca}^{2+}$  fluxes in the root cap in the non-damaging micro-measurement technique (NMT) assay, whereas *PIF3-myc* and Col-0 root caps had a similar net  $\text{Ca}^{2+}$  flux (Figure 5H). In line with the above results, *piezo-1* roots exhibited a penetration defect similar to that seen in *pif3-1* and *fer-4* (Figure 5I). These findings indicate that the FER-PIF3 module regulates *PIEZO* expression in the root cap.

### FER interacts with, phosphorylates, and stabilizes PIF3

To further explore the molecular mechanisms by which the FER pathway modulates root penetration, we tested whether FER interacts with PIF3 in a yeast two-hybrid (Y2H) assay. Indeed, PIF3 interacted with the cytoplasmic domain (CD) of FER, FER-CD (amino acids 469–896, Figure 6A).<sup>54–56</sup> Co-immunoprecipitation (coIP) assays with genetically crossed *FER-GFP* and *PIF3-myc* plants indicated that FER associates with PIF3 *in vivo* (Figure 6B). In agreement with the Y2H and coIP results, GST pull-down experiments also suggested that PIF3-GST can interact with His-tagged kinase domain (KD) of FER (amino acids 518–816, FER-KD) *in vitro* (Figure 6C). As the interaction between the kinase domain and PIF3 raised the possibility that FER might phosphorylate the TF, we performed *in vitro* phosphorylation assays with purified recombinant PIF3-GST, His-FER-KD, and His-FER<sup>K565R</sup>-KD (a kinase-dead FER, as a negative control). As shown in Figure 6D, an antibody against phosphorylated serine residues (anti-pSer/Thr) detected

recombinant PIF3 when PIF3-GST was co-incubated with His-FER-KD (lane 3), but not with the negative control His-FER<sup>K565R</sup>-KD (lane 5). It was possible to detect phosphorylated His-FER-KD in this assay due to its autophosphorylation ability.<sup>57,58</sup> We identified 10 phosphorylation sites (Ser-48, Ser-58, Ser-115, Ser-160, Ser-196, Ser-201, Thr-234, Ser-250, Thr-335, and Thr-499) in this phosphorylation system using liquid chromatography-tandem mass spectrometry (LC-MS/MS; Figures 6E and S6). Notably, 8 of these 10 phosphorylation sites (Ser-48, Ser-115, Ser-160, Ser-196, Ser-201, Thr-234, Thr-335, and Thr-499) were distinct from those known to be targeted by the red-light photoreceptor phytochrome B, phyB,<sup>59</sup> suggesting that FER-dependent phosphorylation of PIF3 may exert a function different from that of phyB. To test whether these phosphorylation sites are required for PIF3 function, we generated transgenic lines in the *pif3-1* background expressing a phospho-mimic version (*pPIF3::PIF3<sup>mut10D</sup>-Venus*, 10 phosphorylation sites mutated to Asp), a non-phosphorylatable version (*pPIF3::PIF3<sup>mut10A</sup>-Venus*, 10 phosphorylation sites mutated to Ala), and wild-type PIF3 variants under the control of the *PIF3* promoter (Figure S7A). Although *PIF3* transcript levels were comparable between *pPIF3::PIF3-Venus*, *pPIF3::PIF3<sup>mut10A</sup>-Venus*, and *pPIF3::PIF3<sup>mut10D</sup>-Venus* (Figure S7B) and *pPIF3::PIF3-Venus* and *pPIF3::PIF3<sup>mut10D</sup>-Venus* transgenes rescued the root penetrating rate of the *pif3-1* mutant (Figure S7C), we failed to identify a transgenic line carrying *pPIF3::PIF3-Venus* or *pPIF3::PIF3<sup>mut10A</sup>-Venus* with strong Venus fluorescence that was comparable to that of *pPIF3::PIF3<sup>mut10D</sup>-Venus*, *Empty vector-Venus*, or *PIF3-GFP* (driven by 35S promoter) seedlings (Figure S7A). To overcome this difficulty, we performed an *in vivo* stability test in the *PIF3-GFP* background using GFP fluorescence intensity as readouts. We determined that FER activation upon RALF1 treatment increases PIF3-GFP abundance and accumulation in the nucleus of root cells (Figure 6F). Another *in vivo* stability test in the *PIF3-myc* also displayed that RALF1 treatment increases PIF3-myc abundance (Figure 6G). To assess whether phosphorylation by FER stabilizes PIF3, we tested the degradation rate of recombinant PIF3 and its phospho-mimic (GST-PIF3<sup>mut10D</sup>) and non-phosphorylatable versions (GST-PIF3<sup>mut10A</sup>) when incubated in total protein lysates prepared from Col-0 roots over 5 min. GST-PIF3<sup>mut10D</sup> displayed a lower degradation rate than GST-PIF3 and GST-PIF3<sup>mut10A</sup>, based on the amount of protein remaining after 5 min (Figure 6H), indicating that phosphorylated PIF3 is more stable. This result may explain why seedlings harboring *pPIF3::PIF3<sup>mut10D</sup>-Venus*, but not *pPIF3::PIF3-Venus*

(B) Root cap phenotype of Col-0, *fer-4*, *pif3-1*, and *PIF3-Venus*. The dashed magenta line indicates the columella root cap (CRC) cells. L, layer.

(C) Cell layer number of the CRC in Col-0, *fer-4*, *pif3-1*, and *PIF3-Venus* (15–21 seedlings of each group).

(D) Root cap sloughing analysis for Col-0, *fer-4*, *pif3-1*, and *pPIF3::PIF3-Venus*. More than 80 roots were counted for each group.

(E) AtPIEZO-NLS-YFP fluorescence intensity in root cap cells after treatment with RALFs. Seedlings grown on solidified half-strength MS medium (control) were treated with water (mock), RALF1, or RALF23 in liquid half-strength medium. Results are shown as boxplots; the edges of the box represent the first and the third quartiles; the center line and vertical line represent the mean and deviation, respectively.

(F) Chromatin immunoprecipitation-quantitative PCR (ChIP-qPCR) analysis of PIF3 binding to the *PIEZO* promoter. ChIP assays were performed using an anti-Myc antibody. Data are mean  $\pm$  SD of three biological replicates.

(G) PIF3 binds to two motifs within the *PIEZO* promoter, as determined by electrophoretic mobility assay (EMSA). See also Table S1. Competitor was unlabeled DNA fragments. The positions of the probes used for the EMSA are shown in (F) in magenta.

(H) Net  $\text{Ca}^{2+}$  fluxes in the root cap cells of Col-0, *fer-4*, *pif3-1*, *PIF3-myc*, and *piezo-1* seedlings that were grown on the medium for 3 days (n = 5 seedlings of each group). The inset diagram indicates the position for  $\text{Ca}^{2+}$  flux measurement using non-damaging micro-measurement technique (NMT).

(I) Penetrating rate of Col-0, *fer-4*, *pif3-1*, and *piezo-1* roots into the medium solidified with 2% agar. Data are mean  $\pm$  SD (n = 3 plates, >20 seedlings of each group). White triangles indicate penetrating roots. Magenta arrows indicate seedlings with nonpenetrating roots. For (A), (C), (E), (F), (H), and (I), data were analyzed by one-way ANOVA with Tukey's test. Different lowercase letters indicate significant difference (p < 0.05).

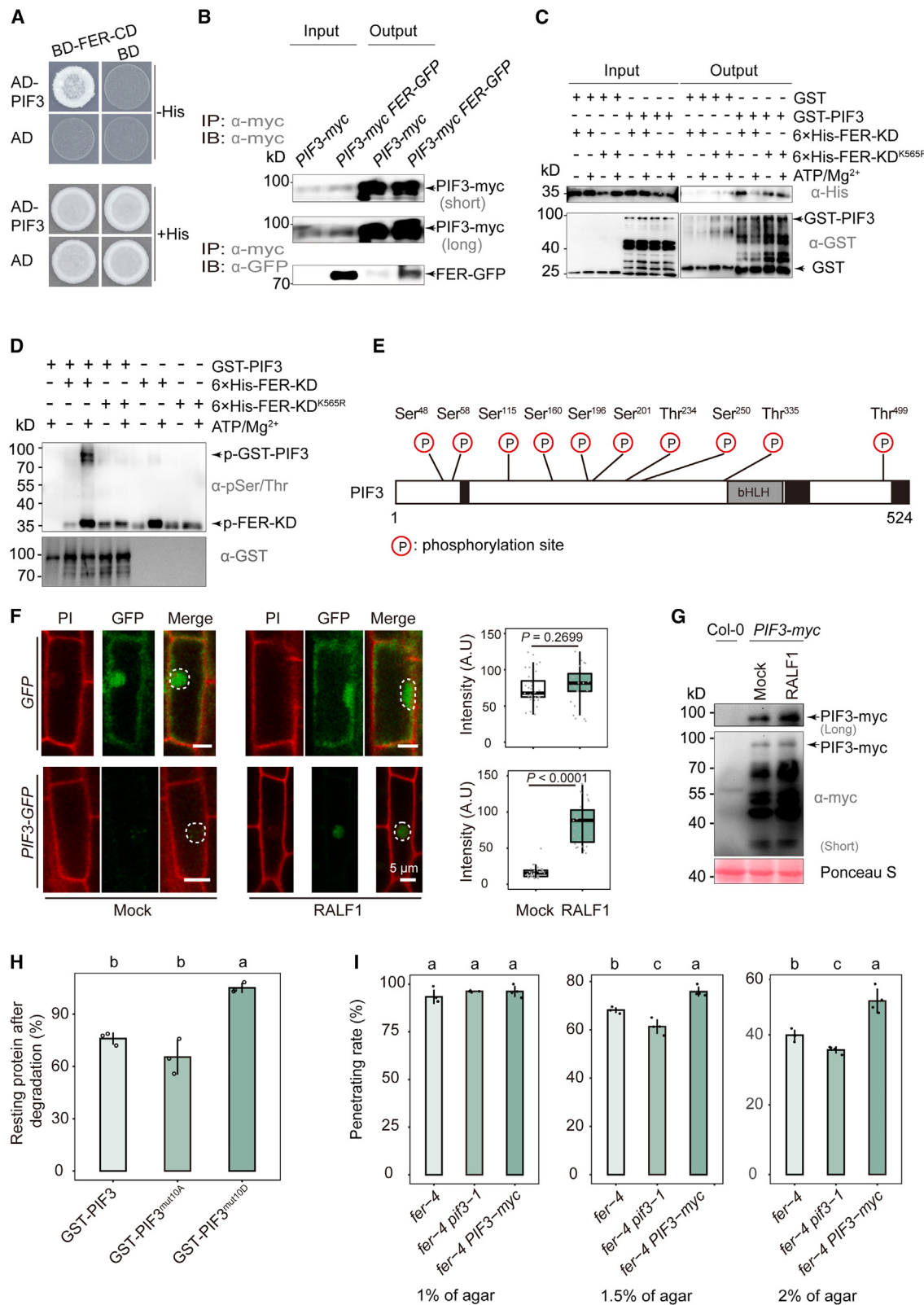


**Figure 6. FER interacts with, phosphorylates, and stabilizes PIF3**

(A) Yeast two-hybrid (Y2H) assays showing the interaction between PIF3 and FER. Synthetic defined medium lacking His (-His) and containing 20 mM 3-amino-1,2,4-triazole (3-AT) was used to test the interaction. PIF3 was cloned into the pGADT7 (AD) vector, and the FER-CD was cloned into the pGKBT7 (BD) vector.

(legend continued on next page)  
Developmental Cell 59, 434–447, February 26, 2024 443

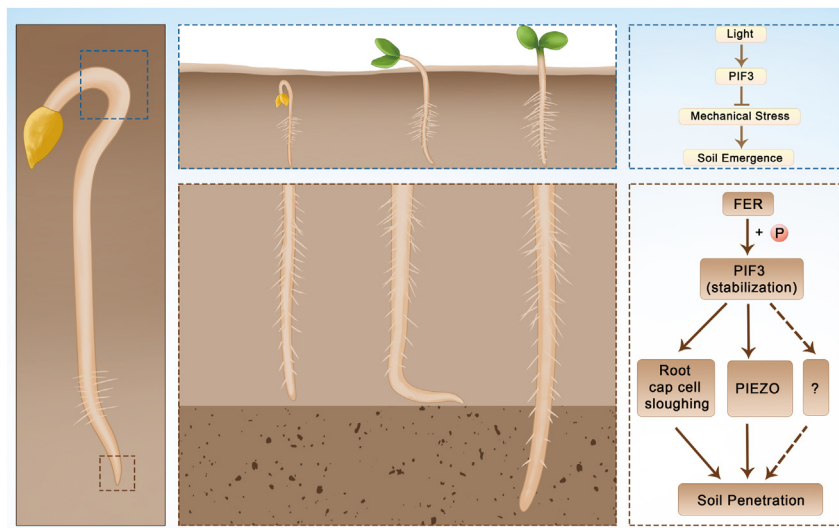


**Figure 7.** A working model for the integrated regulation of the emergence of cotyledons from the soil and root penetration into the soil by PIF3

For cotyledon emergence, PIF3 transduces light signals to control mechanical stress caused by soil covering. For root penetration, PIF3 transfers the soil constraints perceived by FER to the transcriptional machinery to mediate root cap cell sloughing and induce the expression of the mechanosensitive ion channel gene *PIEZO* in the root cap and possibly other unknown factors. In this pathway, FER phosphorylates and stabilizes PIF3, resulting in its higher abundance in the root cap.

or *pPIF3::PIF3<sup>mut10A</sup>-Venus*, displayed detectable Venus signal in root cells (Figure S7A). Given that PIF3 binding to the *PIEZO* promoter was not affected by RALF1 treatment (Figure 5F), we speculate that PIF3 stabilization mainly facilitates *PIEZO* expression in the root cap (Figure 5E). Lastly, *fer-4 PIF3-myc* showed a higher penetration capacity when grown on MS medium solidified with 1.5% and 2% agar than that *fer-4* (Figure 6I). Overexpressing *PIF3* also promoted the growth of the primary root, hypocotyl, petioles, and shoots of *fer-4* (Figures S5C–S5E). The *pif3-1* mutant did not show these effects (Figures S5C–S5E). Collectively, these data indicate that FER physically interacts with, phosphorylates, and stabilizes PIF3.

## DISCUSSION

In nature, plant roots need to overcome physical impedance when penetrating into soil to obtain water and nutrients. Here, we propose a signaling pathway whereby the CWI sensor FER works in concert with the mechanosensitive ion channel *PIEZO* (via PIF3) in roots to perceive soil constraints and modulate soil penetration capacity. Our findings also indicated that the basic helix-loop-helix (bHLH) TF PIF3 unifies two key aspects of seed germination: cotyledon emergence above the soil surface<sup>1–3</sup> and root penetration into the soil (this study, Figure 7).

Both the emergence from and penetration into the soil directly determine nascent seedling growth. Before reaching the soil surface, seedlings prioritize hypocotyl elongation by monitoring the quantity and quality of light via phytochromes. Whether light signaling components are involved in regulating root growth into the deeper soil remains unexplored. We identified here a receptor kinase-TF module that integrates mechanical pressure and darkness signals: In the absence of light, PIF3, probably with a photoreceptor such as phototropin-1,<sup>60</sup> transduces the mechanical signal perceived by FER to the transcriptional level to confer root penetration capacity to *Arabidopsis* seedlings.

The role of FER in mechanical perception and the defect of *fer* mutants in penetrating compacted substrates were previously explored by Shih et al.<sup>29</sup> They provided a mechanism by which FER mediates short-term ion signaling ( $\text{Ca}^{2+}$  and  $\text{H}^+$ , within 60–90 s) and induces the expression of touch-inducible genes (within 20 min) upon root bending and when encountering a physical barrier, subsequently causing spatiotemporal fluctuations of growth within the whole root. Although we set out to investigate the defects of *fer-4* root in penetrating into solidified medium and in root growth, we shed insights into the molecular mechanism behind root penetration into soil. (1) We identified the direct target of FER, the TF PIF3, and its target *PIEZO*. The FER-PIF3-*PIEZO* module executes a long-term (within 5–7 days) program. (2) We established the root cap as the tissue-specific site of mechanical perception. Taken together, Shih et al.<sup>29</sup> and we have jointly shown the essential roles of FER in root penetration into soil.

- (B) Co-immunoprecipitation (coIP) assays with PIF3-myc and FER-GFP, using an anti-myc antibody for the IP. PIF3-myc and FER-GFP were detected using anti-myc and anti-GFP antibodies, respectively.
- (C) GST pull-down assay. Recombinant GST protein and His-FER-KD proteins were detected with anti-GST and anti-His antibodies, respectively.
- (D) *In vitro* phosphorylation assay for recombinant PIF3-GST. The indicated proteins and reagents were mixed and incubated for 30 min. Phosphorylation was detected with an anti-phosphoserine/threonine antibody.
- (E) Diagram of PIF3 with all phosphorylation sites identified. See also Figure S6.
- (F) GFP fluorescence intensity in the nucleus of the root cells for 35S::GFP(GFP) and PIF3-GFP seedlings after treatment with RALF1 for 2 h. Results are shown as boxplots; the edges of the box represent the first and the third quartiles; the center line and vertical line represent the mean and standard deviation, respectively. The p values were obtained by Student's t test. PI, propidium iodide. The nuclei are indicated by the dashed white circles.
- (G) PIF3-myc abundance increases upon treatment with RALF1 for 5 h.
- (H) *In vitro* degradation assay for recombinant PIF3 and variants. GST-tagged protein abundance was determined by the immunoblot analysis. Different lowercase letters indicate significant differences at  $p < 0.05$ .
- (I) Root penetrating rates of the *fer-4*, *fer-4 pif3-1*, and *fer-4 PIF3-myc* seedlings. Data were analyzed by one-way ANOVA with Tukey's test. Different lowercase letters indicate significant differences ( $p < 0.05$ ).

Our findings do not rule out the possibility that root hairs and the cortex also contribute to root penetration. Their roles can be further explored by a deeper analysis of our scRNA-seq data-sets. Given that FER functions in nutrient balancing,<sup>26</sup> osmotic stress,<sup>16</sup> light signaling,<sup>60</sup> and plant-bacteria interactions,<sup>61</sup> future studies should focus on determining whether the FER-mediated penetration pathway steers the direction and depth of root growth via these related pathways.

Root penetration ability, which contributes to deep rooting in plants, is an attractive aim for crop breeding to develop soil compaction-resilient crop varieties. A proper root penetrability may endow plants with plasticity to acclimate to diverse abiotic stresses in soils.<sup>8</sup> Our findings not only improve our understanding of the mechanisms underlying root penetration ability but also will assist breeders in generating germplasm with increased tolerance to the constraints associated with compacted soil.

### Limitations of the study

In this study, we showed that FER-dependent phosphorylation of PIF3 is required for root penetration, involving the transcriptional regulation of a gene encoding a mechanosensitive ion channel and the regulation of root cap sloughing. However, our data suggest that other root penetration related signaling may also participate, as the root penetration phenotype of *fer-4* was more robust than that of *pif3-1* and *piezo-1*. This result suggests that other unidentified signaling components likely function together with the FER-PIF3-PIEZO signaling pathway. Further studies should explore these components and dissect the relationship between the corresponding pathway (e.g., oxygen sensing) and the FER-PIF3-PIEZO signaling pathway.

### STAR★METHODS

Detailed methods are provided in the online version of this paper and include the following:

#### ● KEY RESOURCES TABLE

#### ● RESOURCE AVAILABILITY

- Lead contact
- Materials availability
- Data and code availability

#### ● EXPERIMENTAL MODEL AND STUDY PARTICIPANT DETAILS

- Plants materials and growth conditions

#### ● METHOD DETAILS

- Analysis of soil properties
- Transgenic materials
- Imaging and tissue staining
- Root cap sloughing assay
- X-ray computed tomography
- Protoplasting
- Single-cell RNA-seq data preprocessing
- Gene Ontology (GO) enrichment analysis
- Correlation analysis
- Paired Motif Enrichment Tool analysis
- Integrated Gene Regulatory Network
- Fluorescence intensity measurement
- ChIP-qPCR analysis
- Electrophoretic mobility shift assay (EMSA)

- Measurement of net Ca<sup>2+</sup> fluxes
- Yeast two-hybrid (Y2H) assay
- Recombinant protein production
- Co-immunoprecipitation (coIP) assay
- GST pull-down assay
- *In vitro* phosphorylation assay
- Identification of phosphorylation sites
- *In vivo* PIF3 abundance analysis
- *In vitro* degradation assay

#### ● QUANTIFICATION AND STATISTICAL ANALYSIS

### SUPPLEMENTAL INFORMATION

Supplemental information can be found online at <https://doi.org/10.1016/j.devcel.2024.01.001>.

### ACKNOWLEDGMENTS

The authors are grateful to Meixia Hu and Shufeng Song (State Key Laboratory of Hybrid Rice, Hunan Hybrid Rice Research Center) for their technical support on confocal microscope. We thank Dr. Hongdong Chen (College of Life Sciences, Peking University) for the kind gift of *PIF3-GFP* seeds. Weijun Chen and other members in the laboratory are thanked for critical reading the manuscript and helpful discussions. The sequencing was conducted by OE Biotech Co., Ltd. (Shanghai). X-ray computed tomography imaging was performed at the Analytical Instrumentation Center of Hunan University (Changsha, 410082, China). The work was supported by grants from the National Natural Science Foundation of China (NSFC-32070769 and -32370757), the National Key R&D Program of China (2023YFD1401100), a China Postdoctoral Science Foundation funded project (2020M672475), and the Science and Technology Innovation Program of Hunan Province (no. 2023ZJ1080, 2021JJ10015, and 2021JJ40060).

### AUTHOR CONTRIBUTIONS

F.Y. and F.X. designed the research. F.X., J.C., Y.L., S.O., Y.W., M.Y., and X.F. performed the experiments. F.X., F.Y., and K.H. wrote the manuscript. All authors reviewed and approved the manuscript for publication.

### DECLARATION OF INTERESTS

The authors declare no competing interests.

Received: February 2, 2023

Revised: September 23, 2023

Accepted: January 5, 2024

Published: January 26, 2024

### REFERENCES

1. Liu, X.Q., Liu, R.L., Li, Y., Shen, X., Zhong, S.W., and Shi, H. (2017). EIN3 and PIF3 form an interdependent module that represses chloroplast development in buried seedlings. *Plant Cell* 29, 3051–3067.
2. Shi, H., Liu, R.L., Xue, C., Shen, X., Wei, N., Deng, X.W., and Zhong, S.W. (2016). Seedlings transduce the depth and mechanical pressure of covering soil using COP1 and ethylene to regulate EBF1/EBF2 for soil emergence. *Curr. Biol.* 26, 139–149.
3. Wu, Q.Q., Li, Y., Lyu, M., Luo, Y.W., Shi, H., and Zhong, S.W. (2020). Touch-induced seedling morphological changes are determined by ethylene-regulated pectin degradation. *Sci. Adv.* 6, eabc9294.
4. Zhong, S.W., Shi, H., Xue, C., Wei, N., Guo, H.W., and Deng, X.W. (2014). Ethylene-orchestrated circuitry coordinates a seedling's response to soil cover and etiolated growth. *Proc. Natl. Acad. Sci. USA* 111, 3913–3920.
5. Clark, L.J., Whalley, W.R., and Barraclough, P.B. (2003). How do roots penetrate strong soil? *Plant Soil* 255, 93–104.

6. Iijima, M., Morita, S., and Barlow, P.W. (2008). Structure and function of the root cap. *Plant Prod. Sci.* 11, 17–27.
7. Arnaud, C., Bonnot, C., Desnos, T., and Nussaume, L. (2010). The root cap at the forefront. *C. R. Biol.* 333, 335–343.
8. Bello-Bello, E., López-Arredondo, D., Rico-Chambrón, T.Y., and Herrera-Estrella, L. (2022). Conquering compacted soils: uncovering the molecular components of root soil penetration. *Trends Plant Sci.* 27, 814–827.
9. Bengough, A.G., Loades, K., and McKenzie, B.M. (2016). Root hairs aid soil penetration by anchoring the root surface to pore walls. *J. Exp. Bot.* 67, 1071–1078.
10. Potocka, I., and Szymanowska-Pulka, J. (2018). Morphological responses of plant roots to mechanical stress. *Ann. Bot.* 122, 711–723.
11. Chimungu, J.G., Loades, K.W., and Lynch, J.P. (2015). Root anatomical phenes predict root penetration ability and biomechanical properties in maize (*Zea Mays*). *J. Exp. Bot.* 66, 3151–3162.
12. Schneider, H.M., Strock, C.F., Hanlon, M.T., Vanhees, D.J., Perkins, A.C., Ajmera, I.B., Sidhu, J.S., Mooney, S.J., Brown, K.M., and Lynch, J.P. (2021). Multiseriate cortical sclerenchyma enhance root penetration in compacted soils. *Proc. Natl. Acad. Sci. USA* 118, e2012087118.
13. Franck, C.M., Westermann, J., and Boisson-Dernier, A. (2018). Plant mactein-like receptor kinases: from cell wall integrity to immunity and beyond. *Annu. Rev. Plant Biol.* 69, 301–328.
14. Zhu, S., Fu, Q., Xu, F., Zheng, H., and Yu, F. (2021). New paradigms in cell adaptation: decades of discoveries on the CrRLK1L receptor kinase signalling network. *New Phytol.* 232, 1168–1183.
15. Voxeur, A., and Höfte, H. (2016). Cell wall integrity signaling in plants: "To grow or not to grow that's the question". *Glycobiology* 26, 950–960.
16. Feng, W., Kita, D., Peaucelle, A., Cartwright, H.N., Doan, V., Duan, Q.H., Liu, M.C., Maman, J., Steinhorst, L., Schmitz-Thom, I., et al. (2018). The FERONIA receptor kinase maintains cell-wall integrity during salt stress through  $\text{Ca}^{2+}$  signaling. *Curr. Biol.* 28, 666–675.e5.
17. Lin, W., Tang, W., Pan, X., Huang, A., Gao, X., Anderson, C.T., and Yang, Z. (2022). Arabidopsis pavement cell morphogenesis requires FERONIA binding to pectin for activation of ROP GTPase signaling. *Curr. Biol.* 32, 497–507.e4.
18. Tang, W., Lin, W., Zhou, X., Guo, J., Dang, X., Li, B., Lin, D., and Yang, Z. (2022). Mechano-transduction via the pectin-FERONIA complex activates ROP6 GTPase signaling in Arabidopsis pavement cell morphogenesis. *Curr. Biol.* 32, 508–517.e3.
19. Haruta, M., Sabat, G., Stecker, K., Minkoff, B.B., and Sussman, M.R. (2014). A Peptide hormone and its receptor protein kinase regulate plant cell expansion. *Science* 343, 408–411.
20. Stegmann, M., Monaghan, J., Smakowska-Luzan, E., Rovenich, H., Lehner, A., Holton, N., Belkhadir, Y., and Zipfel, C. (2017). The receptor kinase FER is a RALF-regulated scaffold controlling plant immune signaling. *Science* 355, 287–289.
21. Ge, Z.X., Bergonci, T., Zhao, Y.L., Zou, Y.J., Du, S., Liu, M.C., Luo, X.J., Ruan, H., García-Valencia, L.E., Zhong, S., et al. (2017). Arabidopsis pollen tube integrity and sperm release are regulated by RALF-mediated signaling. *Science* 358, 1596–1600.
22. Mecchia, M.A., Santos-Fernandez, G., Duss, N.N., Somoza, S.C., Boisson-Dernier, A., Gagliardini, V., Martínez-Bernardini, A., Fabrice, T.N., Ringli, C., Muschietti, J.P., et al. (2017). RALF4/19 peptides interact with LRX proteins to control pollen tube growth in Arabidopsis. *Science* 358, 1600–1603.
23. Wang, Y., Coomey, J., Miller, K., Jensen, G.S., and Haswell, E.S. (2022). Interactions between a mechanosensitive channel and cell wall integrity signaling influence pollen germination in *Arabidopsis thaliana*. *J. Exp. Bot.* 73, 1533–1545.
24. Liu, H.B., Li, X., Cai, J., Jiang, L.L., Zhang, X., Wu, D., Wang, L., Yang, A., Guo, C., Chen, J., et al. (2023). A screening of inhibitors targeting the receptor kinase FERONIA reveals small molecules that enhance plant root immunity. *Plant Biotechnol. J.* 21, 63–77.
25. Zhu, S., Estévez, J.M., Liao, H., Zhu, Y., Yang, T., Li, C., Wang, Y., Li, L., Liu, X., Pacheco, J.M., et al. (2020). The RALF1-FERONIA complex phosphorylates eIF4E1 to promote protein synthesis and polar root hair growth. *Mol. Plant* 13, 698–716.
26. Song, L., Xu, G., Li, T., Zhou, H., Lin, Q., Chen, J., Wang, L., Wu, D., Li, X., Wang, L., et al. (2022). The RALF1-FERONIA complex interacts with and activates TOR signaling in response to low nutrients. *Mol. Plant* 15, 1120–1136.
27. Duan, Q.H., Kita, D., Li, C., Cheung, A.Y., and Wu, H.M. (2010). FERONIA receptor-like kinase regulates RHO GTPase signaling of root hair development. *Proc. Natl. Acad. Sci. USA* 107, 17821–17826.
28. Zhu, S.R., Martínez Pacheco, J.M., Estevez, J.M., and Yu, F. (2020). Autocrine regulation of root hair size by the RALF-FERONIA-RSL4 signaling pathway. *New Phytol.* 227, 45–49.
29. Shih, H.W., Miller, N.D., Dai, C., Spalding, E.P., and Monshausen, G.B. (2014). The receptor-like kinase FERONIA is required for mechanical signal transduction in *Arabidopsis* seedlings. *Curr. Biol.* 24, 1887–1892.
30. Fang, X., Liu, B., Shao, Q., Huang, X., Li, J., Luan, S., and He, K. (2021). AtPiezo plays an important role in root cap mechanotransduction. *Int. J. Mol. Sci.* 22, 467.
31. Mousavi, F., Abdi, E., Fatehi, P., Ghalandarzadeh, A., Bahrami, H.A., Majnounian, B., and Ziadi, N. (2021). Rapid determination of soil unconfined compressive strength using reflectance spectroscopy. *Bull. Eng. Geol. Environ.* 80, 3923–3938.
32. Mousavi, S.A.R., Dubin, A.E., Zeng, W.Z., Coombs, A.M., Do, K., Ghadiri, D.A., Keenan, W.T., Ge, C.N., Zhao, Y.D., and Patapoutian, A. (2021). PIEZO ion channel is required for root mechanotransduction in *Arabidopsis thaliana*. *Proc. Natl. Acad. Sci. USA* 118, e2102188118.
33. Rotman, N., Rozier, F., Boavida, L., Dumas, C., Berger, F., and Faure, J.E. (2003). Female control of male gamete delivery during fertilization in *Arabidopsis thaliana*. *Curr. Biol.* 13, 432–436.
34. Li, C., Yeh, F.L., Cheung, A.Y., Duan, Q., Kita, D., Liu, M.C., Maman, J., Luu, E.J., Wu, B.W., Gates, L., et al. (2015). Glycosylphosphatidylinositol-anchored proteins as chaperones and co-receptors for FERONIA receptor kinase signaling in *Arabidopsis*. *eLife* 4, e06587.
35. Wang, D.M., Liang, X.X., Bao, Y.Z., Yang, S.X., Zhang, X., Yu, H., Zhang, Q., Xu, G.Y., Feng, X.Z., and Dou, D.L. (2020). A malectin-like receptor kinase regulates cell death and pattern-triggered immunity in soybean. *EMBO Rep.* 21, e50442.
36. Zhang, X., Wang, D., Chen, J., Wu, D., Feng, X., and Yu, F. (2021). Nematode RALF-Like 1 targets soybean malectin-like receptor kinase to facilitate parasitism. *Front. Plant Sci.* 12, 775508.
37. Bengough, A.G., McKenzie, B.M., Hallett, P.D., and Valentine, T.A. (2011). Root elongation, water stress, and mechanical impedance: a review of limiting stresses and beneficial root tip traits. *J. Exp. Bot.* 62, 59–68.
38. Colombi, T., Kirchgessner, N., Walter, A., and Keller, T. (2017). Root tip shape governs root elongation rate under increased soil strength. *Plant Physiol.* 174, 2289–2301.
39. Roué, J., Chauvet, H., Brunel-Michac, N., Bizet, F., Moulia, B., Badel, E., and Legué, V. (2020). Root cap size and shape influence responses to the physical strength of the growth medium in *Arabidopsis thaliana* primary roots. *J. Exp. Bot.* 71, 126–137.
40. Zheng, G.X.Y., Terry, J.M., Belgrader, P., Ryvkin, P., Bent, Z.W., Wilson, R., Ziraldo, S.B., Wheeler, T.D., McDermott, G.P., Zhu, J.J., et al. (2017). Massively parallel digital transcriptional profiling of single cells. *Nat. Commun.* 8, 14049.
41. Birnbaum, K., Shasha, D.E., Wang, J.Y., Jung, J.W., Lambert, G.M., Galbraith, D.W., and Benfey, P.N. (2003). A gene expression map of the *Arabidopsis* root. *Science* 302, 1956–1960.
42. Brady, S.M., Orlando, D.A., Lee, J.Y., Wang, J.Y., Koch, J., Dinneny, J.R., Mace, D., Ohler, U., and Benfey, P.N. (2007). A high-resolution root spatio-temporal map reveals dominant expression patterns. *Science* 318, 801–806.

43. Zhang, T.Q., Xu, Z.G., Shang, G.D., and Wang, J.W. (2019). A single-cell RNA sequencing profiles the developmental landscape of *Arabidopsis* Root. *Mol. Plant* **12**, 648–660.
44. Cho, H.T., and Cosgrove, D.J. (2002). Regulation of root hair initiation and expansin gene expression in *Arabidopsis*. *Plant Cell* **14**, 3237–3253.
45. De Clercq, I., Van de Velde, J., Luo, X.P., Liu, L., Storme, V., Van Bel, M., Pottie, R., Vaneechoutte, D., Van Breusegem, F., and Vandepoele, K. (2021). Integrative inference of transcriptional networks in *Arabidopsis* yields novel ROS signalling regulators. *Nat. Plants* **7**, 500–513.
46. Rich-Griffin, C., Eichmann, R., Reitz, M.U., Hermann, S., Woolley-Allen, K., Brown, P.E., Wiwatdirekkul, K., Esteban, E., Pasha, A., Kogel, K.H., et al. (2020). Regulation of cell type-specific immunity networks in *Arabidopsis* roots. *Plant Cell* **32**, 2742–2762.
47. Guo, H.Q., Nolan, T.M., Song, G.Y., Liu, S.Z., Xie, Z.L., Chen, J.I., Schnable, P.S., Walley, J.W., and Yin, Y.H. (2018). FERONIA receptor kinase contributes to plant immunity by suppressing jasmonic acid signaling in *Arabidopsis thaliana*. *Curr. Biol.* **28**, 3316–3324.e6.
48. Darwish, E., Ghosh, R., Ontiveros-Cisneros, A., Tran, H.C., Petersson, M., De Milde, L., Broda, M., Goossens, A., Van Moerkercke, A., Khan, K., et al. (2022). Touch signalling and thigmomorphogenesis are regulated by complementary CAMTA3- and JA-dependent pathways. *Sci. Adv.* **8**, eabm2091.
49. Driouich, A., Durand, C., and Vicré-Gibouin, M. (2007). Formation and separation of root border cells. *Trends Plant Sci.* **12**, 14–19.
50. McKenzie, B.M., Mullins, C.E., Tisdall, J.M., and Bengough, A.G. (2013). Root-soil friction: quantification provides evidence for measurable benefits for manipulation of root-tip traits. *Plant Cell Environ.* **36**, 1085–1092.
51. Mravec, J., Guo, X.Y., Hansen, A.R., Schückel, J., Kračun, S.K., Mikkelsen, M.D., Mouille, G., Johansen, I.E., Ulvskov, P., Domozych, D.S., et al. (2017). Pea border cell maturation and release involve complex cell wall structural dynamics. *Plant Physiol.* **174**, 1051–1066.
52. Zhang, Y., Mayba, O., Pfeiffer, A., Shi, H., Tepperman, J.M., Speed, T.P., and Quail, P.H. (2013). A Quartet of PIF bHLH factors provides a transcriptionally centered signaling hub that regulates seedling morphogenesis through differential expression-patterning of shared target genes in *Arabidopsis*. *PLoS Genet.* **9**, e1003244.
53. Radin, I., Richardson, R.A., Coomey, J.H., Weiner, E.R., Bascom, C.S., Li, T., Bezanilla, M., and Haswell, E.S. (2021). Plant PIEZO homologs modulate vacuole morphology during tip growth. *Science* **373**, 586–590.
54. Chen, J., Yu, F., Liu, Y., Du, C.Q., Li, X.S., Zhu, S.R., Wang, X.C., Lan, W.Z., Rodriguez, P.L., Liu, X.M., et al. (2016). FERONIA interacts with ABI2-type phosphatases to facilitate signaling cross-talk between abscisic acid and RALF peptide in *Arabidopsis*. *Proc. Natl. Acad. Sci. USA* **113**, E5519–E5527.
55. Du, C.Q., Li, X.S., Chen, J., Chen, W.J., Li, B., Li, C.Y., Wang, L., Li, J.L., Zhao, X.Y., Lin, J.Z., et al. (2016). Receptor kinase complex transmits RALF peptide signal to inhibit root growth in *Arabidopsis*. *Proc. Natl. Acad. Sci. USA* **113**, E8326–E8334.
56. Kong, Y.Q., Chen, J., Jiang, L.L., Chen, H., Shen, Y.A., Wang, L.F., Yan, Y.J., Zhou, H., Zheng, H.P., Yu, F., et al. (2023). Structural and biochemical basis of *Arabidopsis* FERONIA receptor kinase-mediated early signaling initiation. *Plant Commun.* **4**, 100559.
57. Li, C.Y., Liu, X.M., Qiang, X.N., Li, X.Y., Li, X.S., Zhu, S.R., Wang, L., Wang, Y., Liao, H.D., Luan, S., et al. (2018). EBP1 nuclear accumulation negatively feeds back on FERONIA-mediated RALF1 signaling. *PLoS Biol.* **16**, e2006340.
58. Wang, L., Yang, T., Wang, B.Q., Lin, Q.L., Zhu, S.R., Li, C.Y., Ma, Y.C., Tang, J., Xing, J.J., Li, X.S., et al. (2020). RALF1-FERONIA complex affects splicing dynamics to modulate stress responses and growth in plants. *Sci. Adv.* **6**, eaaz1622.
59. Ni, W.M., Xu, S.L., Chalkley, R.J., Pham, T.N.D., Guan, S.H., Maltby, D.A., Burlingame, A.L., Wang, Z.Y., and Quail, P.H. (2013). Multisite light-induced phosphorylation of the transcription factor PIF3 is necessary for both its rapid degradation and concomitant negative feedback modulation of photoreceptor phyB levels in *Arabidopsis*. *Plant Cell* **25**, 2679–2698.
60. Li, C., Chen, J., Li, X., Zhang, X., Liu, Y., Zhu, S., Wang, L., Zheng, H., Luan, S., Li, J., et al. (2022). FERONIA is involved in phototropin 1-mediated blue light phototropic growth in *Arabidopsis*. *J. Integr. Plant Biol.* **64**, 1901–1915.
61. Song, Y., Wilson, A.J., Zhang, X.C., Thoms, D., Sohrabi, R., Song, S.Y., Geissmann, Q., Liu, Y., Walgren, L., He, S.Y., et al. (2021). FERONIA restricts *Pseudomonas* in the rhizosphere microbiome via regulation of reactive oxygen species. *Nat. Plants* **7**, 644–654.
62. Duan, Q., Kita, D., Johnson, E.A., Aggarwal, M., Gates, L., Wu, H.M., and Cheung, A.Y. (2014). Reactive oxygen species mediate pollen tube rupture to release sperm for fertilization in *Arabidopsis*. *Nat. Commun.* **5**, 3129.
63. Kim, J.Y., Yi, H.K., Choi, G., Shin, B., Song, P.S., and Choi, G.S. (2003). Functional characterization of Phytochrome Interacting Factor 3 in phytochrome-mediated light signal transduction. *Plant Cell* **15**, 2399–2407.
64. Wang, H.P., Li, Y., Pan, J.J., Lou, D.J., Hu, Y.R., and Yu, D.Q. (2017). The bHLH transcription factors MYC2, MYC3, and MYC4 are required for jasmonate-mediated inhibition of flowering in *Arabidopsis*. *Mol. Plant* **10**, 1461–1464.
65. Chen, C.J., Chen, H., Zhang, Y., Thomas, H.R., Frank, M.H., He, Y.H., and Xia, R. (2020). TBtools: an integrative toolkit developed for interactive analyses of big biological data. *Mol. Plant* **13**, 1194–1202.
66. Butler, A., Hoffman, P., Smibert, P., Papalexi, E., and Satija, R. (2018). Integrating single-cell transcriptomic data across different conditions, technologies, and species. *Nat. Biotechnol.* **36**, 411–420.
67. McGinnis, C.S., Murrow, L.M., and Gartner, Z.J. (2019). DoubletFinder: doublet detection in single-cell RNA sequencing data using artificial nearest neighbors. *Cell Syst.* **8**, 329–337.e4.
68. Liao, Y., Smyth, G.K., and Shi, W. (2014). featureCounts: an efficient general purpose program for assigning sequence reads to genomic features. *Bioinformatics* **30**, 923–930.
69. Ryu, K.H., Huang, L., Kang, H.M., and Schiefelbein, J. (2019). Single-cell RNA sequencing resolves molecular relationships among individual plant cells. *Plant Physiol.* **179**, 1444–1456.
70. Macosko, E.Z., Basu, A., Satija, R., Nemesh, J., Shekhar, K., Goldman, M., Tirosh, I., Bialas, A.R., Kamitaki, N., Martersteck, E.M., et al. (2015). Highly parallel genome-wide expression profiling of individual cells using nanoliter droplets. *Cell* **161**, 1202–1214.
71. Haghverdi, L., Lun, A.T.L., Morgan, M.D., and Marioni, J.C. (2018). Batch effects in single-cell RNA-sequencing data are corrected by matching mutual nearest neighbors. *Nat. Biotechnol.* **36**, 421–427.
72. Aran, D., Looney, A.P., Liu, L., Wu, E., Fong, V., Hsu, A., Chak, S., Naikawadi, R.P., Wolters, P.J., Abate, A.R., et al. (2019). Reference-based analysis of lung single-cell sequencing reveals a transitional profibrotic macrophage. *Nat. Immunol.* **20**, 163–172.

## STAR★METHODS

## KEY RESOURCES TABLE

REAGENT or RESOURCE	SOURCE	IDENTIFIER
<b>Antibodies</b>		
Mouse monoclonal anti-His	ABclonal	Cat# AE003; RRID: AB_10896771
Mouse monoclonal anti-myc	Cell Signaling	Cat# 2276; RRID: AB_331783
Mouse monoclonal anti-GST	ABclonal	Cat# AE001; RRID: AB_2770403
Mouse monoclonal anti-GFP	ABclonal	Cat# AE012; RRID: AB_2313773
IgG from mouse serum	Sigma	Cat# A5278; RRID: AB_258232
Anti-Phospho-Serine/Tyrosine	ABclonal	Cat# AP0893; RRID: AB_330301
<b>Bacterial and virus strains</b>		
<i>Saccharomyces cerevisiae</i> : AH109	AXYBIO	Cat# JM-001
<i>Escherichia coli</i> : DH5a	Tsingke	Cat# TSC-C14
<i>Escherichia coli</i> : BL21 (DE3)	Tsingke	Cat# TSC-E06
<i>Agrobacterium tumefaciens</i> : GV3101	Sangon Biotech	Cat# B528430
<b>Chemicals, peptides, and recombinant proteins</b>		
RNasin Ribonuclease Inhibitor	Promega	Cat# N211A
RNase inhibitor	New England Biolabs	Cat# M0314S
Complete™ Protease Inhibitor Cocktail	Roche	Cat# 4693116001
RALF1 and RALF23 peptides	Guoping Yaoye (Anhui) Co., Ltd.	N/A
FER-CD	Kong et al. <sup>56</sup>	N/A
FER-CD <sup>K565R</sup>	Kong et al. <sup>56</sup>	N/A
Murashige and Skoog Medium	Phytotech	Cat# M519
Phytobblend	Caisson Labs	Cat# PTP01
Macerozyme R-10	YAKULT	Cat# L0021
Cellulase R-10	YAKULT	Cat# L0012
Pectolyase	Sigma	Cat# P-3026
Yeast Nitrogen Base	Sangon Biotech (Shanghai) Co., Ltd.	Cat# A610507
PMSF	Solarbio	Cat# P0100-1
MG132	MedChemExpress	Cat# HY-13259
GST beads	Genescrypt	Cat# L00206-50
D-Luciferin	BioVision	Cat# 306
Propidium iodide	Sigma	Cat# 25535-16-4
Calcofluor white	Sigma	Cat# 18909-100ML
NMT microelectrode	Xuyue Science and Technology (Beijing) Co., Ltd.	N/A
Amicon Ultra centrifugal filters (30K MWCO)	Millipore	Cat# UFC9030
Nitrocellulose membrane	PALL	Cat# P-N66485
<b>Critical commercial assays</b>		
Dual Luciferase Reporter Gene Assay Kit	Beyotime	Cat# RG027
SuperScript IV First-Strand Synthesis System	Thermo Fisher Scientific	Cat# 18091050
ChamQTM Universal SYBR qPCR Master Mix	Vazyme Biotech co. Ltd	Cat# Q711-02
TRIzol™ Reagent	Invitrogen	Cat# 15596026
DNase I	Thermo Fisher Scientific	Cat# EN0521
BCA kit	Solarbio	Cat# PC0020-500
Falcon Cell Strainers	Corning	Cat# 352340

(Continued on next page)

**Continued**

REAGENT or RESOURCE	SOURCE	IDENTIFIER
<b>Deposited data</b>		
scRNA-seq data	This paper, <a href="https://www.ncbi.nlm.nih.gov/">https://www.ncbi.nlm.nih.gov/</a>	GEO(GSE225299)
Western blot raw data	This paper; Mendeley	<a href="https://data.mendeley.com/preview/kphx3c9mkd?a=cd326c6-0731-4543-a6ce-0b107397fdcd">https://data.mendeley.com/preview/kphx3c9mkd?a=cd326c6-0731-4543-a6ce-0b107397fdcd</a>
<b>Experimental models: Cell lines</b>		
Arabidopsis: Col-0, <i>fer-4</i> , <i>fer-5</i> , C24, <i>srn</i> , <i>llg1-2</i>	Chen et al. <sup>54</sup> ; Duan et al. <sup>62</sup> ; Li et al. <sup>34</sup>	N/A
Arabidopsis: <i>pif3-1</i> , 35S::PIF3-myc	Kim et al. <sup>63</sup>	N/A
Arabidopsis: <i>piezo-1</i> , <i>piezo-c1</i> , AtPIEZO-NLS-YFP	Fang et al. <sup>30</sup>	N/A
Arabidopsis: PIF3-GFP	Ni et al. <sup>59</sup>	N/A
Arabidopsis: <i>fer-4 pif3-1</i> , <i>fer-4 PIF3-myc</i> , PIF3-myc FER-GFP	This paper	N/A
Arabidopsis: Empty vector-Venus, pPIF3::PIF3 <sup>mut10A</sup> -Venus; pPIF3::PIF3 <sup>mut10D</sup> -Venus	This paper	N/A
Arabidopsis: <i>ddf1</i> , <i>rap2.6</i> , <i>wrky38</i> , <i>wrky45</i> , <i>zat6</i>	Salk Institute, <a href="http://signal.salk.edu">http://signal.salk.edu</a>	<i>ddf1</i> : SALK_127759C, <i>rap2.6</i> : SAIL_1225_G09, <i>wrky38</i> : SAIL_749_B02, <i>wrky45</i> : SALK_210247C, <i>zat6</i> : SALK_061991C
Arabidopsis: <i>myc2myc3</i> , <i>myc2myc4</i> , <i>myc3myc4</i> , <i>myc2myc3myc4</i>	Wang et al. <sup>64</sup>	N/A
Soybean: <i>William82</i> , <i>Gmlmm1-1</i> , <i>Gmlmm1-2</i>	Wang et al. <sup>35</sup>	N/A
<b>Oligonucleotides</b>		
Primers and synthetic RNA sequence list, see Table S1	This paper	N/A
<b>Recombinant DNA</b>		
Plasmid:	This paper	N/A
cDNA: PIF3	Tair; <a href="https://www.arabidopsis.org/">https://www.arabidopsis.org/</a>	PIF3: At1G09530
pGEX-4T-1-PIF3	This paper	N/A
pGEX-4T-1-PIF3 <sup>mut10A</sup>	This paper	N/A
pGEX-4T-1-PIF3 <sup>mut10D</sup>	This paper	N/A
pCambia1300-pPIF3::PIF3-Venus	This paper	N/A
pCambia1300-pPIF3::PIF3 <sup>mut10A</sup> -Venus	This paper	N/A
pCambia1300-pPIF3::PIF3 <sup>mut10D</sup> -Venus	This paper	N/A
pGADT7-PIF3	This paper	N/A
<b>Software and algorithms</b>		
Fiji	NIH	<a href="https://imagej.net/ImageJ">https://imagej.net/ImageJ</a>
TBtools V 1.0983	Chen et al. <sup>65</sup>	<a href="https://github.com/CJ-Chen/TBtools-II">https://github.com/CJ-Chen/TBtools-II</a>
R software V 4.3.2	The R Foundation	<a href="https://www.r-project.org">https://www.r-project.org</a>
Fluxes V2.0	Younger USA LLC, Amherst, MA, USA	
Cell Ranger 6.1.2	10x Genomics	<a href="https://support.10xgenomics.com/single-cell-gene-expression/software/pipelines/latest/what-is-cell-ranger">https://support.10xgenomics.com/single-cell-gene-expression/software/pipelines/latest/what-is-cell-ranger</a>
Seurat version 3.1.1	Butler et al. <sup>66</sup>	<a href="https://satijalab.org/seurat/">https://satijalab.org/seurat/</a>
DoubletFinder 2.0.3	McGinnis et al. <sup>67</sup>	<a href="https://github.com/chris-mcginnis-ucsf/DoubletFinder">https://github.com/chris-mcginnis-ucsf/DoubletFinder</a> <a href="https://doi.org/10.1101/j.cels.2019.03.003">https://doi.org/10.1101/j.cels.2019.03.003</a>
featureCounts v2.0.1	Liao et al. <sup>58</sup>	<a href="http://subread.sourceforge.net/">http://subread.sourceforge.net/</a>

(Continued on next page)

**Continued**

REAGENT or RESOURCE	SOURCE	IDENTIFIER
ggplot2 v3.3.5	The R Foundation	<a href="https://cran.r-project.org/web/packages/ggplot2/index.html">https://cran.r-project.org/web/packages/ggplot2/index.html</a>
MEME	NIH	<a href="http://meme-suite.org/">http://meme-suite.org/</a>
Prism	GraphPad Software	<a href="https://www.graphpad.com/features">https://www.graphpad.com/features</a>
MaxQuant (version 1.6.1.0)	Thermo Fisher Scientific	N/A
Proteome Discoverer (version 1.4)	Thermo Fisher Scientific	N/A
<b>Other</b>		
Confocal microscope LSM880 and LSM980	Carl Zeiss, Jena, Germany	N/A
Arabidopsis Information Resource (TAIR)	N/A	<a href="https://arabidopsis.org">https://arabidopsis.org</a>
Micro penetrometers	Changzhou Baling Future Intelligent Technology Co., LTD	WXGR-3.0 and WXGR-2.0
Microscope Leica DM500	Leica Co., LTD	N/A
X-ray microscopy	Carl Zeiss, Jena, Germany	Xredia 515 Versa
Non-invasive Micro-test system	NMT150S, Younger USA LLC, Amherst, MA, USA	N/A

**RESOURCE AVAILABILITY****Lead contact**

Further information and requests for resources and reagents should be directed to and will be fulfilled by the lead contact, Feng Yu ([feng\\_yu@hnu.edu.cn](mailto:feng_yu@hnu.edu.cn)).

**Materials availability**

All plant materials generated in this study are available from the [lead contact](#) with a completed materials transfer agreement.

**Data and code availability**

The scRNA-seq data was deposited in NCBI with the accession number “GSE225299” ([key resources table](#)). Original western blot images reported in this paper will be shared by the [lead contact](#) upon request. This paper does not report original code. Any additional information required to reanalyze the data reported in this paper is available from the [lead contact](#) upon request. Some of the raw data for western blots have been uploaded to Mendeley at <https://data.mendeley.com/preview/kphx3c9mkd?a=cdf326c6-0731-4543-a6ce-0b107397fdcd>.

**EXPERIMENTAL MODEL AND STUDY PARTICIPANT DETAILS****Plants materials and growth conditions**

Arabidopsis (*Arabidopsis thaliana*) accession Columbia-0 (Col-0) was used as the wild type in this study. Forty milliliters of half-strength Murashige and Skoog (MS) medium (Murashige and Skoog basal salt mixture) containing 1%, 1.5%, or 2% (w/v) of phytoagar was poured into a 100 × 100 × 15-mm Petri plate. After it had solidified, the MS medium was cut along a straight line with a sharp sterile blade about 2 cm from the plate edge, and the smaller segment was removed. Arabidopsis seeds were surface-sterilized with 15% (v/v) NaClO for 5 min and then stratified for 2 d at 4 °C in darkness to break dormancy before sowing. The plates were placed vertically at a constant temperature of 22 °C under a long-day (16-h light/8-h dark) photoperiod for 7 d. Seeds were placed on the cut surface at the middle of section (2 mm in thickness). Seedlings whose roots grew into the medium were counted as penetrating, or as nonpenetrating otherwise.

Concerning the Arabidopsis seedlings growth on sand, river sand (Xiangjiang, Changsha, Hunan) (diameter 250 µm–1 mm [> 98%], 1–3 mm [< 2%]) was sterilized and mixed with Agra-perlite (grain 2.0–3.0 mm) at a 9:1 ratio (w/w) and placed in round Petri dishes (125 mm in diameter). The sand was sterilized by autoclaving at 120°C for 5 h before being pre-soaked with sterilized liquid half-strength MS medium. Seven-day-old seedlings grown on half-strength MS solidified medium were transferred to sand plates (containing a 2-cm layer of sand) and allowed to grow for another 7 d. The growth conditions were the same as above.

The soybean (*Glycine max*) cultivar ‘Williams 82’, and the *Gmlmm1-1* and *Gmlmm1-2* mutants were a kind gift from Daolong Dou.<sup>35</sup> Soybean seeds were placed on uncompacted soil and watered once daily. Seeds were germinated at 28°C before being moved to uncompacted or compacted soil. A layer of uncompacted soil (~5 mm in height) was placed on the soil surface to cover the seeds. After 5 d of growth, the soil around the seedlings was removed gently and root penetration was scored. To observe soybean root hair, soybean seeds were surface sterilized with 75% (v/v) ethanol for 4 min and 30% (v/v) NaClO for 40 min. The seeds were allowed to soak in distilled water for 8 h. The seeds were placed on wet filtering paper at 37°C for 12 h and transferred to 22°C for 36 h.

### METHOD DETAILS

#### Analysis of soil properties

For the penetration impedance of soil and sand, micro penetrometers were used. At least three replicates per soil or sand samples were measured.

#### Transgenic materials

For Arabidopsis transgenic lines, the coding sequences of *PIF3* variants (*PIF3<sup>mut10A</sup>* and *PIF3<sup>mut10D</sup>*) were synthesized by Qsingke Company. The coding sequences of *PIF3*, *PIF3<sup>mut10A</sup>*, and *PIF3<sup>mut10D</sup>* were cloned individually into the *EcoRI* and *BamHI* restriction sites of pCambia-1300, in-frame and upstream of the *Venus* sequence. *PIF3* and its variants were placed under the control of the *PIF3* promoter. *FER-GFP* was cloned into the plant expression vector pDT7 with *SpeI* and *PacI* enzymes to generate overexpression plants. Transgenic plants were generated by Agrobacterium (*Agrobacterium tumefaciens*)-mediated transformation of the *pirf3-1* mutant. Primary transformants ( $T_1$ ) were selected based on hygromycin resistance, and  $T_2$  lines containing only one T-DNA insertion were selected for characterization by determining the Mendelian segregation ratio (3:1) of hygromycin-resistant seedlings in the  $T_2$  progeny, which was confirmed in the  $T_3$  progeny. A homozygous *FER-GFP* line was crossed to a *PIF3-myc* line.  $T_2$  progeny were selected based on resistance to basta and kanamycin and verified by immunoblot using anti-GFP and anti-myc antibodies.

#### Imaging and tissue staining

Arabidopsis seedlings grown *in vitro* were fixed overnight in a fixation solution (50% [v/v] methanol, 50% [v/v] acetic acid). Seedlings were then incubated in hot ethanol for 15 min (80% [v/v] ethanol at 80°C) and rehydrated in 50% (v/v) and then 30% (v/v) ethanol for 10 min each. Seedlings were rinsed in distilled water and then incubated in 0.2 M sodium hydroxide containing 1% (w/v) SDS for 30 min at room temperature. Samples were then rinsed in water and stained for 30 min in 1% (v/v) calcofluor white to which a few drops of 10 M sodium hydroxide were added to achieve complete dissolution. Seedlings were then rinsed in water and gently mounted onto a slide to avoid squashing the root tips. Samples were excited at 405 nm with an emission band of 410–550 nm with a Zeiss LSM880 confocal microscope using a 40× objective and a GaAsP spectral detector.

Soybean root hairs were visualized and counted with a microscope (Leica DM500).

#### Root cap sloughing assay

Surface-sterilized Arabidopsis seeds were sown on half-strength MS medium solidified with 1.5% agar (w/v) and allowed to grow for 6 d. Ten minutes before observation under the microscope, 15 μM propidium iodide (PI) solution was sprayed onto the surface of the medium very gently. The solidified medium around the root tip was cut, flipped over, and placed onto a microscope slide.

#### X-ray computed tomography

Soybean seedlings were grown in soil with an uncompacted or compacted (0.7 g/mL) layer. The roots of 7-day-old soybean seedlings were imaged non-destructively in the soil using Xredia 515 Versaat Analytical Instrumentation Center of Hunan University (Changsha, 410082, China). Scans were acquired at 110 kV X-ray energy in normal mode (Objector = 0.4×, exposure time = 3 s, Filter = Air, bin = 2). Scan resolution was 50 μm. Three-dimensional image reconstruction was performed using Scout-and-Scan Control System software. Dragonfly V4.2 was used to segment the roots from the soil.

#### Protoplasting

Seeds of the Arabidopsis accession Columbia-0 (Col-0) and the *fer-4* mutant were surface sterilized with 15% (v/v) NaClO, sown onto agar plates containing solidified half-strength MS medium (pH 5.8, 0.8% [w/v] sucrose, 1% [w/v] phytoagar), and grown vertically at 22°C in long-day conditions (16-h light/8-h darkness). The roots of 7-day-old seedlings were treated with liquid half-strength MS medium (pH 5.8, 0.8% [w/v] sucrose) containing 2 μM synthesized RALF1 peptide for 2 h. To expose the roots to treatment and to avoid light, a piece of filter paper (1.5 × 8 cm) was soaked in liquid medium containing RALF1 and placed on top of the roots. Approximately 3,000 treated roots were excised approximately 1.5 cm from their tip, broadly sliced with a scalpel, and then passed through a 70-μm cell strainer above the 35-mm well of a six-well plate containing 8% (w/v) mannitol. After rinsing out the debris corresponding to solidified medium, the root fragments were treated with 10 mL protoplasting solution optimized for scRNA-seq from a previously described protocol.<sup>69</sup> Immediately before use, the enzyme solution was prepared (1.25% [w/v] cellulase 0.1% [w/v] pectolyase, 8% [w/v] mannitol, 20 mM MES [pH 5.7], 20 mM KCl, 10 mM CaCl<sub>2</sub>, and 0.1% [w/v] bovine serum albumin). The enzyme solution was activated by heating at 55°C for 10 min. The plate was shaken at 90 rpm for 1 h at 25°C, and then the cell solution was centrifuged at 300 g for 10 min at 25°C and the pellet was resuspended in 500 μL washing solution (8% [w/v] mannitol, 20 mM MES pH 5.7, 20 mM KCl, 10 mM CaCl<sub>2</sub>, and 0.1% [w/v] bovine serum albumin [BSA]). The cell suspension was centrifuged again at 100g for 6 min at 25°C, the entire procedure was repeated twice. All resuspended protoplasts were filtered through a 40-μm cell strainer. The supernatant was discarded and the cells collected by the cell strainer were resuspended with 100 μL of 8% (w/v) mannitol. Eighteen microliters of resuspended protoplasts were mixed with 2 μL of 0.4% (w/v) trypan blue. The stained protoplasts were observed under a microscope, and four photographs were taken for each sample. The living and stained protoplasts and debris were counted and the

protoplast density, cell viability, and debris rate were calculated. The cell number was adjusted to ~1,000 cells/ $\mu$ L as recommended by the Chromium 10 $\times$  Genomics manual. The protoplast suspension was loaded into a Chromium microfluidic chip with 30 v2 chemistry and barcoded with a 103 Chromium Controller (10 $\times$  Genomics).

### Single-cell RNA-seq data preprocessing

The Cell Ranger software pipeline (version 3.1.0) provided by 10 $\times$  Genomics was used to demultiplex cellular barcodes, and map reads to the *Arabidopsis* genome BSgenome object ("BSgenome. *Athaliana*. TAIR. TAIR9") with the TAIR10 gene annotation file using the STAR aligner; reads were down-sampled reads as required to generate normalized aggregate data across samples, producing a matrix of gene counts for each cell. The unique molecular identifier (UMI) count matrix was processed using the R package Seurat version 3.1.1.<sup>66</sup> To remove low-quality cells and likely multiple captures, which is a major concern in microdroplet-based experiments, any cell whose UMI/gene number fell within mean  $\pm$  2 standard deviations was removed, assuming a Gaussian distribution of UMI/gene numbers for each cell. Following visual inspection of the distribution of mitochondrial genes expressed in each cell, low-quality cells were further discarded where >10 % of the counts belonged to mitochondrial genes. After applying these quality control criteria, approximately 13,000 single cells were retained for downstream analyses. Library size normalization was performed with the NormalizeData function in Seurat<sup>66</sup> to obtain normalized counts. Specifically, the global-scaling normalization method "Log-Normalize" was used to normalize the gene expression measurements for each cell by the total expression levels, multiplied by a scaling factor (10,000 by default), and the results were log transformed.

The top variable genes across single cells were identified using the method described previously.<sup>70</sup> The most variable genes were selected using the FindVariableGenes function (mean.function = ExpMean, dispersion.function = LogVMR) in Seurat.<sup>66</sup> To remove the batch effects in scRNA-seq data, the mutual nearest neighbor method<sup>71</sup> was applied with the R package batchelor. Cells were visualized using 2D following dimensionality reduction according to their gene expression profile using the FindClusters function in Seurat<sup>66</sup> with t-Distributed Stochastic Neighbor Embedding (t-SNE) and Uniform Manifold Approximation and Projection (UMAP) algorithm with the RunTSNE and RunUMAP functions in Seurat, respectively. The FindAllMarkers function (test.use = bimod) in Seurat<sup>66</sup> was used to identify marker genes for each cluster. For a given cluster, FindAllMarkers identified positive markers<sup>72</sup> compared to all other cells.

Differentially expressed genes (DEGs) were identified using the FindMarkers function (test.use = MAST) in Seurat.<sup>66</sup>  $P$  value < 0.05 and  $|\text{Log}_2[\text{fold-change}]| > 0.58$  were set as the thresholds for significant differential expression. Gene ontology (GO) term enrichment and Kyoto Encyclopedia of Genes and Genomes (KEGG) pathway enrichment analysis of DEGs were performed using R, based on the hypergeometric distribution.

### Gene Ontology (GO) enrichment analysis

GO term enrichment analysis was performed using Metascape (<https://metascape.org/gp/index.html#/main/step1>) and the R package ClusterProfiler (with default parameters). DEGs of the columella root cap, lateral root cap\_a, lateral root cap\_b, and root hairs were used in Metascape to identify enriched GO terms. The same DEGs were used in ClusterProfiler to select the genes regulated by MYC (MYC2, MYC3, and MYC4) and PIF (PIF3, PIF4, PIF5, and PIF7) transcription factor families. The threshold adjusted  $P$ -value was < 0.05. All genes in the *Arabidopsis* genome were used as background. Fisher's exact test was used, and the false discovery rate (FDR) was calculated for multiple test correction. Enriched GO terms were determined for biological processes, molecular functions, and cellular components.

### Correlation analysis

For correlation analysis of merged single-cell and bulk RNA-seq data,  $\text{Log}_2$  (mean RPM+1) expression values for each gene from two replicates of pooled scRNA-seq and bulk RNA-seq were quantile-normalized, and the Pearson's-correlation coefficient was calculated in R. For correlation analysis between scRNA-seq replicates, each replicate was simulated as a bulk RNA-seq sample, the  $\text{Log}_2$  (mean RPM+1) expression values were calculated for all genes, and the Pearson's correlation coefficient between replicates was calculated in R. For correlation analysis between the scRNA-seq replicates across individual clusters, the average expression of cells within a cluster was calculated for each replicate using the Seurat command Average Expression (object, use.raw = T). The Pearson's-correlation coefficient between the replicates was then determined for each cluster using Seurat CellPlot.

### Paired Motif Enrichment Tool analysis

Pairs of TF binding motifs was identified with the Paired Motif Enrichment Tool (PMET) ([http://nero.wbsc.warwick.ac.uk/tools/user\\_case\\_form.php](http://nero.wbsc.warwick.ac.uk/tools/user_case_form.php)). The gene IDs from TAIR for the above-mentioned DEGs in each cell type were uploaded to the online tool. Parameters were as follows: promoter length = 1,000, max motif matches = 5, number of selected promoters/intervals = 5,000, 5'-UTR included, potential overlapped promoter removed. All significant motif pairings with adjusted  $P$ -value (Bonferroni) < 0.05 were chosen.

### Integrated Gene Regulatory Network

TF genes associated with DEGs in each cell type were analyzed at <http://bioinformatics.psb.ugent.be/webtools/iGRN/> with a set  $q$ -value < 0.001. The overlapping TFs between iGRN and PMET were identified with TBtools.

### Fluorescence intensity measurement

To measure *PIEZO* expression in the root cap, 7-day-old *Arabidopsis pAtPiezo::NLS-YFP* seedlings grown on half-strength MS medium solidified with 1.5% agar (w/v) were moved to half-strength liquid MS medium containing 1 μM synthesized RALF1 or RALF23 peptide. Seedlings were incubated at a constant temperature of 22 °C for 5 h. For the PIF3 stability test in root cells, 7-day-old *35S::GFP*<sup>58</sup> and *PIF3-GFP*<sup>59</sup> seedlings grown on half-strength solidified MS medium were moved to half-strength liquid MS medium containing 1 μM synthesized RALF1 peptide. Seedlings were incubated in the dark for 2 h. The epidermal cells of roots were observed with an excitation at 488 nm and an emission band of 500–530 nm with a Zeiss LSM880 confocal microscope using a 40× objective and a GaAsP spectral detector. To quantify the relative fluorescence intensity of YFP or GFP, all images were captured using the same laser, pinhole, and gain settings of the confocal microscope to allow comparison of the data. Fiji software was used to quantify the fluorescence intensity in all images.

### ChIP-qPCR analysis

Two grams of 5-day-old, etiolated Col-0 and *PIF3-myc* (in the Col-0 background) seedlings were cross-linked in 20 mL 1% (v/v) fresh formaldehyde solution under vacuum twice for 8 min each. To quench the cross-linking, 2 M glycine was added to a final concentration of 0.125 M and was applied under vacuum for 5 min. All vacuum steps were performed at -0.08 MPa. Nuclei were pelleted by centrifugation at 4,000 g for 20 min at 4 °C, washed with nuclei extraction buffer 2 (10 mM Tris-HCl pH 8.0, 0.25 M sucrose, 10 mM MgCl<sub>2</sub>, 1% [v/v] Triton X-100, 0.1 mM PMSF and protease inhibitor), and lysed in nuclei lysis buffer (50 mM Tris-HCl, pH 8.0, 10 mM EDTA, 1% [w/v] SDS, 0.1 mM PMSF and 1:100 [v/v] protease inhibitor cocktail). Chromatin was sheared by sonication (220 W, 20 min, 4 s sonicating plus 9 s break) to approximately 500 bp fragments. The chromatin solution was diluted 10-fold with ChIP dilution buffer (16.7 mM Tris-HCl, pH 8.0, 167 mM NaCl, 1.1% [v/v] Triton X-100, 1.2 mM EDTA, 0.1 mM PMSF, and 1:100 [v/v] protease inhibitor cocktail). Myc magnetic beads (3 μL per IP) were washed with ChIP dilution buffer two times, mixed with the chromatin solution and incubated at 4°C overnight. Immuno-complexes were precipitated and washed with four different buffers: low-salt buffer (20 mM Tris-HCl, pH 8.0, 150 mM NaCl, 0.2% [w/v] SDS, 0.5% [v/v] Triton X-100, and 2 mM EDTA), high-salt buffer (20 mM Tris-HCl, 500 mM NaCl, 0.2% [w/v] SDS, 0.5% [v/v] Triton X-100, and 2 mM EDTA pH 8.0), LiCl washing buffer (20 mM Tris-HCl, pH 8.0, 0.25 M LiCl, 1% [v/v] NP-40, 1% [w/v] sodium deoxycholate, and 1 mM EDTA, pH 8.0) and TE washing buffer (10 mM Tris-HCl pH 8.0, and 1 mM EDTA pH 8.0). The bound chromatin fragments were eluted with the elution buffer (50 mM Tris-HCl, pH 8.0, 10 mM EDTA, pH 8.0, and 1% [w/v] SDS) and the cross-linking was reversed by incubating at 65°C overnight. The mixture was treated with proteinase K for 1 h at 45°C to remove proteins. DNA was extracted with phenol/chloroform/isoamyl alcohol (25:24:1, v/v/v) and precipitated with two volumes of 100% ethanol at -80°C for 4 h. To recover the DNA, the sample was centrifuged at 16,000 g for 20 min at 4°C. The pellet was dried briefly and resuspended in 25 μL TE buffer for quantitative PCR analysis.

### Electrophoretic mobility shift assay (EMSA)

Recombinant PIF3-GST protein and GST protein were used for EMSA (see below for production and purification). The probes used for the assays were synthesized and labeled with fluorescein isothiocyanate (FITC, Table S1). The DNA-PIF3 binding reaction consisted of 100 pg probe, 200 ng PIF3-GST protein, 10 mM Tris-HCl, pH 7.5, 5% (v/v) glycerol, 1 mM MgCl<sub>2</sub>, 50 mM KCl, 0.2 mg/mL bovine serum albumin, 0.5 mM dithiothreitol, 0.5 mg/mL polyglutamate, and the indicated amount of unlabeled competitor. The reactions were incubated at room temperature for 30 min and separated by electrophoresis in a 6% (w/v) polyacrylamide gel (acrylamide:bisacrylamide, 29:1) containing 10% (v/v) glycerol, 89 mM Tris-HCl, pH 8.0, 89 mM boric acid, and 2 mM EDTA. The FITC signal was detected using a KODAK 4000MM Image Station.

### Measurement of net Ca<sup>2+</sup> fluxes

The Non-invasive Micro-test Technology (NMT) assay was performed as described previously.<sup>30</sup> Briefly, the net fluxes of Ca<sup>2+</sup> were measured non-invasively with a Non-invasive Micro-test system and with Fluxes V2.0 software. *Arabidopsis* seedlings were grown on medium for 3 days before being transferred to the measurement solution (0.1 mM KCl, 0.1 mM CaCl<sub>2</sub>, 0.1 mM MgCl<sub>2</sub>, 0.5 mM NaCl, 0.3 mM MES, 0.2 mM Na<sub>2</sub>SO<sub>4</sub>, pH 6.0). Calibration solution 1 (0.1 mM KCl, 0.02 mM CaCl<sub>2</sub>, 0.1 mM MgCl<sub>2</sub>, 0.5 mM NaCl, 0.3 mM MES, and 0.2 mM Na<sub>2</sub>SO<sub>4</sub>, pH 6.0) and calibration solution 2 (0.1 mM KCl, 1 mM CaCl<sub>2</sub>, 0.1 mM MgCl<sub>2</sub>, 0.5 mM NaCl, 0.3 mM MES, and 0.2 mM Na<sub>2</sub>SO<sub>4</sub>, pH 6.0) were used for correction. To avoid the interference caused by sloughing cells, the probe was positioned close to the lateral root cap instead of at the tip of the columella root cap. Ion flux recordings were taken over at least 8 min for each root cap with the recorded data during the first minute not considered for calculations. At least 4 plants were measured.

### Yeast two-hybrid (Y2H) assay

Y2H assays were performed as previously described.<sup>14,54</sup> Briefly, the *PIF3* coding sequences were cloned in vector pGADT7 (AD). Primers for cloning are listed in Table S1. The sequence encoding the kinase domain of FER was cloned into pGBK7 (BD). Distinct plasmid pairs were transformed into yeast AH109 cells. The transformants were diluted and plated onto synthetic defined (SD) medium lacking tryptophan and leucine (-Trp-Leu) and SD medium lacking tryptophan, leucine, and histidine (-Trp-Leu-His) but containing 20 mM 3-amino-1,2,4-triazole for 7 d to test the interaction.

### Recombinant protein production

*PIF3* variants (*PIF3*<sup>mut10A</sup> and *PIF3*<sup>mut10D</sup>) were synthesized by Qsingke Company. The coding sequence of *PIF3* and variants were cloned individually into the pGEX-4T-1 plasmid using restriction sites *Eco*RI and *Bam*HI. The resulting constructs were transformed into *Escherichia coli* BL21 star cells. Single clones were picked and transferred to LB medium for overnight culture at 37°C with shaking at 250 rpm. The cultures were diluted 1:50 with fresh LB medium containing 50 mg mL<sup>-1</sup> ampicillin for growth until reaching an optical density at 600 nm (OD<sub>600</sub>) of 0.8. Protein production was induced with 0.5 mM isopropyl-β-D-thiogalactopyranoside (IPTG) at 16°C overnight. The cell cultures were spun down at 5,000 rpm for 8 min at 4°C, and the cell pellet was resuspended in lysis buffer (25 mM Tris-HCl, pH 7.5, 300 mM NaCl, 20 mM imidazole, and 1 mM PMSF) and lysed with an ultrasonic cell disruptor (220 W, 20 min, 4 s sonicating plus 9 s break) on ice. The lysates were centrifuged at 12,000 g for 10 min at 4°C, and the resulting supernatant was transferred to another tube and incubated with Ni-NTA resin at 4°C for 3 h. The Ni-NTA beads were washed extensively with wash buffer (20 mM Tris-HCl, pH 7.5, 300 mM NaCl, and 30 mM imidazole); the recombinant proteins were eluted with elution buffer (20 mM Tris-HCl, pH 7.5, 300 mM NaCl, and 300 mM imidazole). The eluates were desalted via centrifugation with a salt-free buffer (50 mM HEPES-NaOH, pH 7.5) using Amicon Ultra centrifugal filters. The centrifugation step was repeated five times to remove 99.9% of salts. The protein concentration was measured using a BCA kit according to the user manual. Aliquots of GST-*PIF3*, GST-*PIF3*<sup>mut10A</sup>, and GST-*PIF3*<sup>mut10D</sup> proteins were then stored in 50 mM HEPES-NaOH, pH 7.5, at -80 °C until use.

### Co-immunoprecipitation (coIP) assay

For the *in vivo* coIP assay, 5-day-old etiolated *PIF3-myc FER* -GFP seedlings were collected to obtain the protein lysate as above. Myc magnetic beads (50 µL per IP) were washed with Co-IP buffer (50 mM Tris-HCl, pH 7.5, 150 mM NaCl, 1 mM EDTA, 5% [v/v] glycerol, and protease inhibitor mixture containing 1% [v/v] Triton X-100, 1 mM PMSF and 50 µM MG132) two times and then mixed with the lysate and incubated at 4°C for 4 h. Anti-GFP and anti-myc antibodies were used for the immunoblot assay.

### GST pull-down assay

Recombinant His-FER-KD and PIF3-GST proteins were co-incubated with 50 µL of glutathione-agarose beads in binding buffer (50 mM Tris-HCl, pH 8.0, 150 mM NaCl, and 10 mM MgCl<sub>2</sub>) at 4°C for 6 h. The beads were washed with washing buffer I (50 mM Tris-HCl, pH 8.0, 300 mM NaCl, and 0.5% [v/v] Triton X-100) for 10 min and then two times with washing buffer II (50 mM Tris-HCl, pH 8.0, 150 mM NaCl, and 10 mM MgCl<sub>2</sub>), each for 20 min. The proteins on the beads were eluted by boiling in SDS loading buffer, separated by SDS-PAGE, and detected by immunoblotting using an anti-GST or anti-His antibody.

### In vitro phosphorylation assay

An *in vitro* phosphorylation assay was performed as previously described<sup>54,56</sup> with minor modifications. Recombinant FER-KD and FER-KD<sup>K565R</sup> mutant proteins that were co-expressed with λ-PP were purified. FER-KD or FER-KD mutant protein (1 µM) was co-incubated with recombinant PIF3-GST at room temperature for 40 min in 50 µL of assay kinase buffer containing 1 mM ATP and 10 mM Mg<sup>2+</sup>. Proteins were resolved by SDS-PAGE and transferred to a nitrocellulose membrane for protein immunoblotting using anti-phosphothreonine, anti-phosphoserine, and anti-phosphotyrosine antibodies.

### Identification of phosphorylation sites

After phosphorylation by FER-KD, the PIF3-GST bands were excised and cut into small pieces after Coomassie Brilliant Blue staining. Then, the gel pieces were dehydrated, and the proteins were reduced, alkylated, digested, and analyzed by mass spectrometry (MS) as described previously.<sup>58</sup> For label-free quantification, raw files were processed using MaxQuant and Proteome Discoverer. PIF3 phosphopeptides were identified by searching all tandem MS spectra against the Araport11\_pep\_201606 sequence database and filtering using an FDR of < 0.01 at the peptide level and < 0.05 at the protein level by MaxQuant. Carbamidomethylation of cysteines was selected as the fixed modification and oxidation (M) and phosphorylation (STY) were used as variable modifications. In addition, Proteome Discoverer was used to assess phosphorylation localization. After identification, PIF3 protein label-free quantitation of phospho-peptides was performed with the MaxLFQ algorithm integrated in the MaxQuant software suite.

### In vivo PIF3 abundance analysis

Col-0 and *PIF3-myc* seeds were surface sterilized, stratified, and sown on agar plates containing half-strength MS medium solidified with 1.5% agar (w/v) before being placed vertically at 22°C in long-day conditions for 2 d. The seedlings were moved to darkness for 3 d, and incubated with half-strength liquid MS medium containing 1 µM synthesized RALF1 for 5 h. Approximately 1 g of seedlings was ground in liquid nitrogen and then resuspended in coIP buffer (50 mM Tris-HCl, pH 7.5, 150 mM NaCl, 1% [v/v] NP-40, 0.25% [w/v] sodium deoxycholate, 5% [v/v] PPVP, 10% [v/v] glycerol, and 10 mM MgCl<sub>2</sub>). The PIF3-myc protein was visualized by immunoblotting.

### In vitro degradation assay

Total proteins were extracted by homogenizing the roots of 7-day-old Col-0 seedlings in the presence of 150 mM NaCl, 12.5 mM citric acid, and 50 mM Na<sub>2</sub>HPO<sub>4</sub>, pH 6.5 (500 µL of extraction buffer per g tissue). The homogenate was incubated for 1 h on ice. The homogenate was centrifuged at 12,400 g for 10 min at 4°C, and the supernatant was collected. This centrifugation step was repeated twice. Protein concentration was determined in supernatants using the Bradford protein assay method. Equal amounts

of protein samples (2 mg total proteins) were mixed with 200 µg GST-PIF3, GST-PIF3<sup>mut10A</sup>, or GST-PIF3<sup>mut10D</sup> proteins. The protein mixtures were incubated at 22°C for 5 min. The GST-tagged proteins were visualized by immunoblotting with an anti-GST antibody. The gray intensity value of the bands was used to calculate the relative protein abundance. Fiji software was used to quantify band intensities.

#### **QUANTIFICATION AND STATISTICAL ANALYSIS**

Measurements were statistically analyzed in R and Rstudio and plots were created with the ggplot2 package. The data are shown as means ± standard deviation (sd). Significant differences were determined using one-way ANOVA or a least significant difference test, with \* $P < 0.05$ , \*\* $P < 0.01$ , \*\*\* $P < 0.001$ , n.s., not significant. The sample number (n) are indicated in the bar graph or in the legends. All data generated were from independent biological replicates, each measured in technical duplicate or triplicates.